Exploring the use of active microwave resonators for stored-product insect detection

by

Alex Reimer

A Thesis submitted to the Faculty of Graduate Studies of

THE UNIVERSITY OF MANITOBA

in partial fulfilment of the requirements of the degree of

MASTER OF SCIENCE

Department of Physics and Astronomy

University of Manitoba

Winnipeg

Abstract

New sensors are presented which have as their central component an active microwave resonator. The active microwave resonators are planar and contain an active component which compensates for energy loss in the resonator. The result is a very narrow transmission or output spectrum which responds to changes in the immediate proximity of the sensor. This sensor is applied to stored-product insect detection. The ability of the sensor to detect insects both outside and inside individual grain kernels is demonstrated. The sensor is also able to detect insects in small samples of grain, which means it could potentially be used to monitor grain bins for infestations. A technique is proposed which analyses the signal from the sensor to provide an indication of insect presence, and the technique is used to characterize the detection efficiency of the sensor for internal *Sitophilus oryzae* in wheat kernels at different developmental stages.

Contents

List of Figures

Acknowledgements

First, I thank my supervisor Dr. Can-Ming Hu, for the support and instruction he has provided me over the course of my Master's studies. His guidance kept me on course in the numerous instances where I felt lost. He has been a model after whom I could shape my approaches to critical thinking, to effective communication, to project management, and to leadership.

I also owe a debt of gratitude to Dr. Yongsheng Gui, who has taught me so much about all aspects of research work. From proposal writing, to experimental design, to set-up construction, to data collection and analysis, and finally to writing professional scientific reports, he has been an invaluable help at every step leading up to and including this thesis.

I thank the rest of the Dynamic Spintronics group for their generous support and warm friendship.

I thank Drs. Paul Fields and Fuji Jian for their interest in my work and for embarking on this new inter-disciplinary collaboration with me and the Dynamic Spintronics Group. They have broadened my perspective of science and the scientific method.

I give special thanks to the members of my personal life, who have made the stresses of my studies so much easier to bear: to my parents, Brian and Jacqueline, my sister Rhéanne, and my extended family for their love, support, and friendship; to my friends, for their companionship and helping me make the most of my leisure time; and finally to my beloved Laura, who has brought love and light to my every day.

1

INTRODUCTION

1.1 Background

This thesis reports the use of active microwave resonators as sensors in the application of stored-grain insect detection. These resonators are constructed from microstrip, a type of planar transmission line. Because microstrip line is constructed on open planar surfaces, signals propagating along it consist of electromagnetic fields largely situated in open air, making it possible to perform measurements of objects by probing them with the fields. With a resonator, measurements can be made of objects by placing them in the electric field and recording the change in the frequency response of the resonator. In the application of stored-grain insect detection, the presence of insects is indicated by shifts in the resonance frequency, which are caused by the movement of the insects through the electric field of the resonator. This detection technique is also applicable when the insects are moving among grains in a small sample, because the fields penetrate the grains and can probe the interior of the sample volume. As is demonstrated in this thesis, insects both outside and inside the kernels can be detected with this technique.

Grain storage is a vital component of the food production chain, but it is also a significant point of quantitative and qualitative product loss. Across the world, the most significant

cause of loss in storage is infestation by insects [1]. Insects cause quantitative grain loss by consuming the product, and qualitative grain loss by contaminating the product with insect fragments and frass. To make matters worse, insects will also affect the storage micro-climate by creating hotspots and increasing the humidity, which can promote the growth of fungi and micro-organisms, leading to increased product loss [2]. Effective insect management is hindered by the mobility and small size of insects, making them difficult to spot and contain. Furthermore the rapid life-cycles and the large number of offspring produced by insect pests can make even small populations of insects dangerous to stored grains if they are not monitored and controlled.

Critical to effective insect pest management is the monitoring of insect populations in grain stores and shipments. Insect population data can be the deciding factor in whether the expense of fumigation is necessary, or whether a facility should accept a grain shipment. Often, such data are obtained by retrieving a number of representative samples from the bulk. Several retrieval methods exist for this purpose, such as deep-bin cups, probe traps, and vacuum probes [2]. In general, sampling requires manual labour to retrieve and inspect the sample, incurring both a financial cost as well as a safety risk to workers, as sample retrieval often involves climbing storage bins, especially on farms. Once the sample has been retrieved, an estimate of the insect population can be made by counting the insects in the samples. To be counted, the insects in the sample must be separated from the grain (unless they have been retrieved from a trap), and this is usually done by shaking out the insects with a sieve or by using a Berlese funnel. In Berlese funnel technique, a quantity of grain to be tested is placed in a funnel and slowly heated from above by a lamp. The heat forces insects to escape towards the bottom, where they are captured by a dish for later counting. The process takes several hours, with longer times leading to better efficiency [3], but it cannot detect internal insects [4].

Internal insects — insects living inside individual grain kernels — are much more difficult to separate from grain and count. Internal insects are usually larvae who, until they

grow into adults and emerge, will remain inside the kernel. These internal infestations are often nearly impossible to identify by visual inspection; to attempt it would be prohibitively lengthy. As a result, the ability to detect internal insects is of significant interest to researchers, farmers, and grain handlers. Several techniques have demonstrated the ability to detect internal insects. Examples of such techniques include acoustic detection, electrical conductance, NMR spectroscopy, kernel staining, cracking-flotation, near infra-red reflectance (NIR) spectroscopy, and x-ray imaging. A brief description of each approach is given below.

The acoustic detection method [5] uses the sounds produced by insect activity as an indicator of insect presence. This is achieved by recording the sounds captured by a microphone placed in the grain bulk. The presence of insects is then determined either by listening to the recording or by analysing the oscillogram or spectrogram of the recording [6]. The sounds produced by settling grains can also confound the signal. Since it depends on insect movement, this technique cannot detect the presence of eggs or dead insects, and has difficulty detecting small larvae and pupae.

In the electrical conductance technique, insect presence is ascertained by measuring the conductance or resistance of kernels [7]. The voltage across a kernel is measured while it is being crushed, and because insects have a much higher moisture content than sound kernels, infested kernels can be distinguished from sound ones by the measured voltage. This technique is able to detect insects at the larval, pupal, and adult stages in wheat kernels. A method which uses a conductive roller mill to increase throughput has also been demonstrated [8]. The disadvantages of the electrical conductance technique are that it cannot detect insects that have died and dried out, and it cannot detect eggs.

The NMR spectroscopy technique uses the differences in water and lipid content between infested and sound kernels to detect insects. It has been demonstrated to be effective in detecting *Sitophilus granarius* in wheat kernels, but is not effective if the insects have not reached the third instar [9].

Infested kernels can sometimes be identified by staining the kernels: some insects (particularly *Sitophilus* spp.) deposit their eggs in holes chewed in kernels and plug the holes with a gelatinous secretion. These plugs are coloured differently than the rest of the kernel by the application of certain dyes, and it is by the different colouration of these plugs that infested kernels are identified [2]. Examples of dyes used are fuchsin, iodine, and gentian violet. The disadvantage of staining and inspecting the kernels is that it is time consuming and labour intensive.

There are multiple ways to perform the the cracking-flotation technique [2]. The method approved by the American Association of Cereal Chemists [10] is as follows: a grain sample is coarsely ground to liberate the insects from the grain. In the process, the insects are sometimes also ground into pieces. To separate the insect fragments from the grain, the ground sample is mixed with isopropanol and heptane. The heptane is insoluble in isopropanol and forms a layer which floats on the surface. While the grain sinks, insect fragments float and are collected by the heptane layer, which is then separated and filtered so insect fragments can be inspected and counted. Though this technique is effective at detecting insects, it is time consuming and labour intensive.

Near infra-red reflectance spectroscopy is a technique commonly used in grain quality laboratories [2]. It measures absorption spectrum of kernels for radiation wavelengths between 780 nm and 2500 nm to determine if they are infested. The differences in absorption spectra correspond to differences in chemical composition between infested kernels and sound ones. This technique is able to detect both live and dead insects at the larval, pupal, and adult stages in wheat kernels. Automated systems using this technique have been developed [11]. However, it is not effective at detecting low levels of infestation and is sensitive to the moisture content of the kernels, making complex calibrations necessary and frequent [4].

X-rays can be used to produce images of insects hidden inside kernels, which can then identified visually from the radiograph by a human operator [12] or by a neural network analysis [13]. X-ray techniques are most effective at detecting adults, pupae, and large

larvae, and less effective at detecting eggs and small larvae. To increase throughput, grains can be spread into a single layer to image multiple kernels at once. The major drawbacks with this technique are the high energy demand of X-ray systems and the fact that X-rays are ionizing radiation and so may be subject to government regulation and require special operator training.

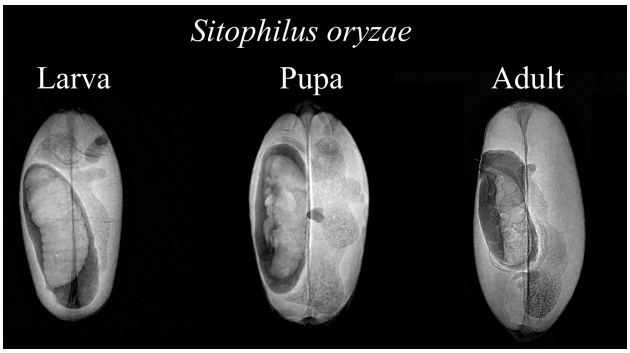

Figure 1.1: X-ray radiographs of *Sitophilus oryzae* inside wheat kernels. These images were produced at the University of Manitoba

Another approach to detecting insects not listed above is microwave radar. This was the first approach at stored-grain pest detection attempted by our group. Until we had been aware of the pest detection problem, we had been developing a life-detection radar system which used a meta-material-based receiving antenna [14]. This radar system used the precise phase measurement of reflected microwaves to detect breathing and heartbeat patterns in radar signals, and was originally pursued as a potential tool for search-and-rescue operations because microwaves can penetrate through many common building materials. Since grains consist of dielectric material, they are to a certain degree penetrable by microwaves. As an initial attempt at pest detection, we used a vector network analyser (VNA) to measure the phase of 4.9 GHz microwaves in a bistatic[1] radar system directed at *Tenebrio molitor* adults contained in a dish located 45 cm from the antennas. Figure 1.2 compares the time-domain signal phase when there were 1 and 5 insects in the dish to when there were no insects in the dish. The presence of *T. molitor* had a clear effect on the signal.

[1]A bistatic radar system is one in which separate antennas transmit and receive the radar signal. It contrasts with a monostatic system, in which a single antenna both transmits and receives the radar signal.

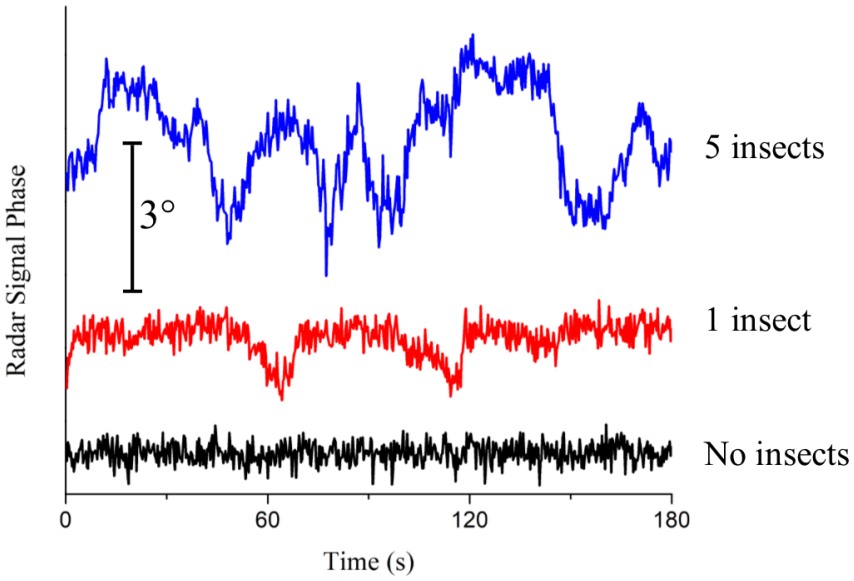

Figure 1.2: The phase of the reflected 4.9 GHz radar signal when directed at *T. molitor* adults in a dish. These measurements demonstrated that radar detection was possible with insects at least as large as *T. molitor*. However, this technique was not successful in detection smaller and more common pest insects such as *C. ferrugineus*.

Despite its success in detecting *T. molitor* adults, the radar approach would not be useful if it could not detect more common pest insects such as *Sitophilus oryzae* or *Cryptolestes ferrugineus*. *Tenebrio molitor* is a relatively large insect (almost 2 cm long), so it is easily separated from grain samples, making sophisticated separation techniques unnecessary. Furthermore, it is only a secondary pest; it feeds on fungus or on grain that has already been damaged. Therefore, *T. molitor* generally does not by itself present a risk to grain stores. Instead, to be most useful, the detection system had to be able to detect primary pests, such as *Triboleum castaneum*, *C. ferrugineus*, and *S. oryzae*, which feed directly on stored grain and diminish its quantity and quality. Therefore, we turned the focus of the radar system tests on *S. oryzae*. The results of these tests were discouraging, as the strength of the signal reflected from *S. oryzae* was so weak that it was difficult to identify any signature of their activity. This is likely due to the fact that, for the microwave frequencies we were able to generate with our equipment at the time, the radar cross section of the insects was very small because of the small insect size compared to the wavelength of the microwaves. If this system

could not detect external adults, it was unlikely that it would be able to detect relatively stationary internal insects. However, the shortcomings of our radar system do not preclude the possibility of using radar to detect stored-product insects. In fact, stored-product insect detection with radar has been achieved elsewhere with higher microwave frequencies (24 GHz) using the Doppler effect[15]. Radar detection of insects at 24 GHz may likely be easier than at lower microwave frequencies because insects have a larger radar cross-section at this frequency, so the reflected signal is stronger [16].

Concurrently with our radar system tests, our group was studying the use of active feedback resonators in a separate research project to study magnon-photon interactions [17]. We noticed that the resonance frequency of these resonators was very sensitive to its surroundings – just walking a few feet from the resonator would perturb the resonance if the resonator was not well shielded. It then occurred to us attempt to detect insects using these resonators. We were encouraged by reports of the detection of single yeast cells achieved using microwave resonators [18]. Active microwave resonators had also been reported to be useful as filters in communication systems because they exhibit such a narrow resonance [19], and as non-contact fluid sensors because of the high resolution afforded by their narrow resonances [20]. Early on, we were met with success in using active microwave resonators to detect stored-grain insects. The following chapters report the work that has followed since.

1.2 Thesis Outline

The objective of this thesis is to present the new sensors and the work we have done to demonstrate their capabilities and potential. In Chapter 2, the theory of operation of the sensors is described, beginning with a review of transmission line theory. A more focussed discussion is then given on a specific type of transmission line, the microstrip line, because it is from microstrip that the sensors are constructed. At this point, there is an aside to review scattering-parameters, which are a key element of the measurement techniques used in the

presented work. Then, a description of microstrip resonators is provided, which is useful in describing the mechanism of the sensors. The chapter concludes with a description of active resonators and the conditions necessary to produce active resonance.

Chapter 3 presents an article we submitted to *Biosystems Engineering* in October 2017 which is currently under review. The article demonstrates the ability of the sensor to detect external insects, *Tribolium castaneum* and *Cryptolestes ferrugineus* adults. This demonstration is done in steps: first, it is confirmed that the presence of insects produces a response in the sensor; second, it is shown how the sensor response varies according to insect activity; third, the demonstration is concluded with a test that shows how the sensor can detect insects in a small sample of wheat and therefore potentially be used to monitor larger grain bulks.

Chapter 4 reports the work we did to demonstrate the detection of internal *Sitophilus oryzae* in wheat kernels. We show how we observed that there is a clear difference between the sensor response to infested kernels and the response to sound kernels. It is then described how *S. oryzae* produces patterns in the sensor response which appear to be unique for each developmental stage. A demonstration is then given of the analysis technique we use to automatically ascertain the presence of insects from the recorded sensor signal which is based on thresholding the first time derivative.

Chapter 5 summarizes the thesis and provides an outlook on this research project.

2

THEORY

In this chapter, the theoretical basis for the description of the active resonator sensors presented in Chapters 3 and 4 is reviewed. The chapter begins with a review of transmission line theory, with an emphasis on microstrip line. The transmission line theory is necessary to explain the operation of microstrip resonators and subsequently the active resonator sensors used in the work presented in this thesis. A description of S-parameters, which are used in our measurements, is also provided.

2.1 Microwave Transmission Lines

2.1.1 General Transmission Lines

Microwave signals have wavelengths roughly ranging from tens of centimetres to a few millimetres. Because microwave transmission lines are at least comparable in length to the wavelength of the signal they carry, the variations in electrical parameters along the length of the line must be considered when analysing or designing them. This is a contrast to DC systems where wave effects can largely be ignored and the electrical parameters can be treated as lumped elements.

Transmission lines consist of at least two conductors and may also comprise dielectric (insulating) material such as plastic, ceramic, or air. Generally, they transport electromagnetic energy via single *transverse electromagnetic* (TEM) mode propagation. In these ways, they are distinct from hollow waveguides, which are composed of a single conductor and therefore can only support TE (transverse electric) and TM (transverse magnetic) modes; they do not support TEM modes. Because they lack a separate internal conductor, hollow waveguides lack the means to carry electric current required to form closed loops of the magnetic field in the transverse plane, as required by Ampère's Law [21]. Furthermore, because TEM fields have the same transverse spatial dependence as static fields, transmission lines are not restricted to being treated as a boundary value problem in the way hollow waveguides are, and instead they can be analysed as distributed parameter networks[1] [22].

When considering a transmission line as a distributed-parameter network, its electrical parameters are treated as per-unit-length quantities. In the analysis, four parameters are considered: the series inductance per unit length, L, which accounts for energy stored in the magnetic field; the capacitance per unit length, C, which accounts for energy stored in the electric field; the series resistance in the conductors per unit length, R, which accounts for resistive loss in the conductors; and the shunt conductance per unit length, G, which accounts for loss in the dielectric.

The four parameters of the transmission line are considered on a small length, Δz, of transmission line, such as in Figure 2.1a, which has an equivalent circuit comprising L, C, R, and G, as shown in Figure 2.1b. To determine the line parameters, we consider the fields – which are fully transverse in the quasi-static approximation – in a cross-section of the transmission line as shown in Figure 2.1c.

Below is a list of the expressions for the parameters L, C, R, and G in terms of the fields of the transmission line.

[1] In microwave technology nomenclature, the term "network" is a general term for a microwave system which may be composed of any combination of circuits, components, and transmission lines. Microwave circuits are a subset of microwave networks. The connecting terminals of a network are called "ports".

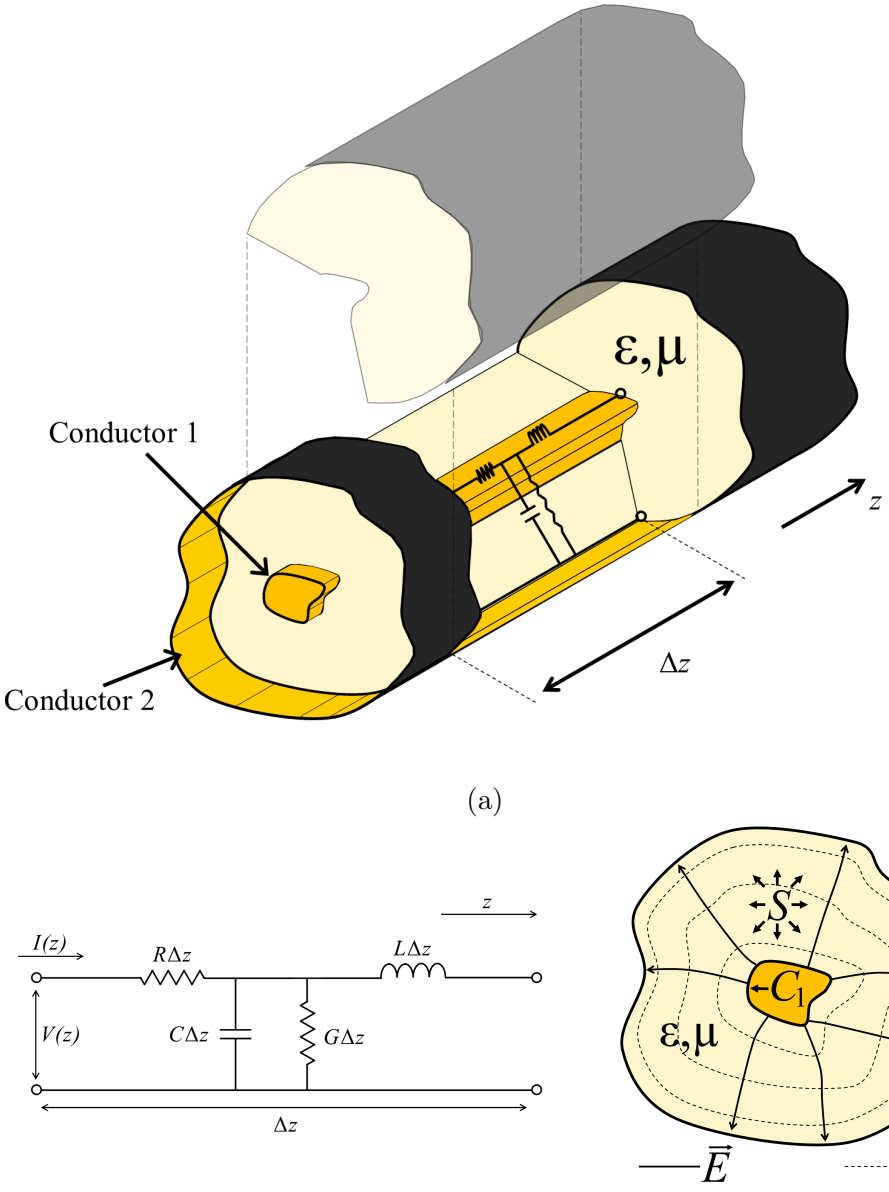

Figure 2.1: An arbitrary two-conductor transmission line can be treated as a distributed parameter network.

In a transmission line, the voltage, $V(z)$, and the current, $I(z)$, can be shown to travel as waves along the transmission line [21, 22]. For simplicity, let us consider the case where the voltage and current waves travel in only one direction; that is, $V(z) = V_0 e^{\pm\gamma z}$ and $I(z) = I_0 e^{\pm\gamma z}$, where γ is the *propagation constant*, which is discussed later.

The inductance L is determined from the time-averaged magnetic energy per unit length in the transmission line, which is stored in the magnetic field, $\vec{H}$, as shown in Figure 2.1c. The resulting expression for L is

$$L = \frac{\mu}{|I_0|^2} \int_S \vec{H} \cdot \vec{H}^* ds, \tag{2.1}$$

where μ is the relative permeability of the dielectric and has a value very close to 1 in most non-ferromagnetic materials. The integral is computed over the entire cross-sectional surface, S, between the conductors. The asterisk (*) denotes the complex conjugate of $\vec{H}$.

Similarly to the determination of L, C is determined from the time-averaged electric energy energy per unit length in the transmission line, which is stored in the electric field, $\vec{E}$, as shown in Figure 2.1c

$$C = \frac{\epsilon'}{|V_0|^2} \int_S \vec{E} \cdot \vec{E}^* ds, \tag{2.2}$$

where ϵ' is the real part of the complex permittivity, $\epsilon = \epsilon' + j\epsilon''$ ($j = \sqrt{-1}$) and relates to the ability of the dielectric to store electric energy. Again, the integral is computed over the surface S.

The resistance, R, accounts for ohmic loss in the conductors. At high frequencies, current is concentrated near the surface of the conductors. Therefore, to get an expression for R, we integrate the power loss due to the surface resistance in the conductors. The result is

$$R = \frac{R_s}{|I_0|^2} \oint_{C_1+C_2} \vec{H} \cdot \vec{H}^* dl, \tag{2.3}$$

where R_s is the surface resistance of the two conductors (assuming they are made of identical

materials) and depends on the skin depth and conductivity of the conductors. The integral is over the closed curves C_1 and C_2 defining the boundaries of each conductor, as shown in Figure 2.1c.

The shunt conductace G accounts for the fraction of the electric energy that is lost in the dieletric. The expression for G, then, is

$$G = \frac{\omega \epsilon''}{|V_0|^2} \int_S \vec{E} \cdot \vec{E}^* ds, \tag{2.4}$$

where $\omega = 2\pi f$ is the angular frequency of the wave and ϵ'' is the imaginary part of the complex permittivity ϵ and relates to the rate at which the dielectric dissipates energy.

The above equations are valid provided that the dielectric is non-dispersive [2] and linear and that the waves propagate in fully TEM modes [22]. In treating the fields $\vec{E}$ and $\vec{H}$ as completely transverse, some assumptions have been implicitly made about the transmission line. First, it was ignored that there is a a longitudinal component of the waves arising from the non-zero surface resistance of the conductors [22]. That said, in most practical transmission lines the conductor resistance is small enough to make the TEM mode a close approximation of the wave. Second, it was assumed that the dielectric is homogeneous in the transverse plane, which is a necessary condition for TEM mode propagation because it ensures that the phase velocity is uniform across a cross-section of the transmission line. If the phase velocities at two points in the transverse plane are different, there must be a longitudinal component to the wave [21, 23].

Now that the parameters L, C, R, and G have been defined, their effects on signal propagation can be discussed. In general, sinusoidal voltage and current waves travelling along

[2] In a non-dispersive medium, the propagation speed of a wave does not depend on its frequency.

a transmission line (along the z-axis) can be expressed by

$$V(z) = V_0 e^{\pm \gamma z}, \tag{2.5a}$$

$$I(z) = I_0 e^{\pm \gamma z}, \tag{2.5b}$$

where a negative exponent represents propagation in the $+z$ direction and a positive exponent represents propagation in the in the $-z$ direction, and γ is the *propagation constant*, with

$$\gamma = \sqrt{(R + j\omega L)(G + j\omega C)} = \alpha + j\beta. \tag{2.6}$$

Here, the real part of γ, α, is the *attenuation coefficient*, and the imaginary part, β is the *phase change coefficient*. The coefficient β gives the phase shift of the wave per unit length of the transmission line, and α gives the wave amplitude decay per unit length of the transmission line. From Eqs. (2.5) and (2.6), we see that the amplitude of a wave is proportional to $e^{-\alpha z}$ in a lossy line. In a lossless line, where R and G are zero, $\alpha = 0$ and $\gamma = j\beta = j\omega\sqrt{LC}$, so the wave amplitude is constant and the wave only undergoes a change in phase as it propagates. Since β relates to the phase change over distance, it can be related to the wavelength on the line, λ, by

$$\lambda = \frac{2\pi}{\beta}. \tag{2.7}$$

The coefficient β is also related to the phase velocity, v_p, by

$$v_p = \frac{\omega}{\beta} = \lambda f. \tag{2.8}$$

The attenuation coefficient, α, is more difficult to generalize than β because there are usually multiple forms of loss in a transmission line and each depend on the specific con-

struction of the line. The coefficient α is then the sum of all dissipative losses, which can include dielectric, conductive, and radiation loss, among other forms.

Another important transmission line constant is the *characteristic impedance*, Z_0. It is given in terms of L, C, R, and G by

$$Z_0 = \sqrt{\frac{R + j\omega L}{G + j\omega C}}. \tag{2.9}$$

Z_0 has units of Ω/m, and, like the other transmission line parameters, is a per-unit-length quantity. It gives the ratio of the voltage wave amplitude to the current wave amplitude. Z_0 is of particular importance when connecting a transmission line to a microwave network because, in order to minimize reflections and maximize power delivery, the characteristic impedance of the line must match the input impedance of the network.

The impedance is an important parameter to consider when connecting transmission lines (or any networks). If the impedances of two transmission lines are mismatched, signals will reflect at the interface of the two lines with a magnitude dependant on the mismatch of the impedances. If we consider a transmission line with impedance Z_1 connected to a second transmission line having an impedance Z_2, then the reflection coefficient of voltage waves for signals travelling from the first to the second line is

$$\Gamma_{12} = \frac{Z_2 - Z_1}{Z_2 + Z_1} = \frac{V_1^r}{V_1^i}, \tag{2.10}$$

where V_1^i is the voltage amplitude of the wave coming from transmission line 1, and V_1^r is the amplitude of the wave reflected at the boundary. The reflection coefficient of waves travelling in the opposite direction is

$$\Gamma_{21} = \frac{V_2^r}{V_2^i} = \frac{Z_1 - Z_2}{Z_1 + Z_2} = -\Gamma_{12}, \tag{2.11}$$

where the same notation is used as in Eq. (2.10).

From the above equations, we see that minimum reflection is achieved when $Z_1 = Z_2$.

This concept applies generally to any interface between microwave networks. In many cases, the reflection coefficient at the input port of a network will also include secondary reflections within the network, and not just the reflections at the interface. The combined result of all reflections is accounted by a single input reflection coefficient, Γ_{in}, which corresponds to a similarly derived input impedance, Z_{in}.

In some situations, such as when constructing resonators, it is useful to terminate a transmission line with an open end or a short-circuit. A short-circuit presents an impedance of 0; therefore, by Eq. (2.10), signals incident on the termination will see a $Z_2 = 0$ and $\Gamma = -1$, corresponding to a total reflection with an inversion of the wave (i.e. a phase shift of π). Conversely, an open end presents an infinite impedance, so $\Gamma \to 1$, corresponding to a total reflection of the wave without inversion (no shift in phase).

2.1.2 Microstrip Transmission Lines

In the work presented in this thesis, extensive use is made of *microstrip* transmission lines. Microstrip transmission line consists of a conducting strip separated from a conducting ground plane by a dielectric layer, as seen in Figure 2.2.

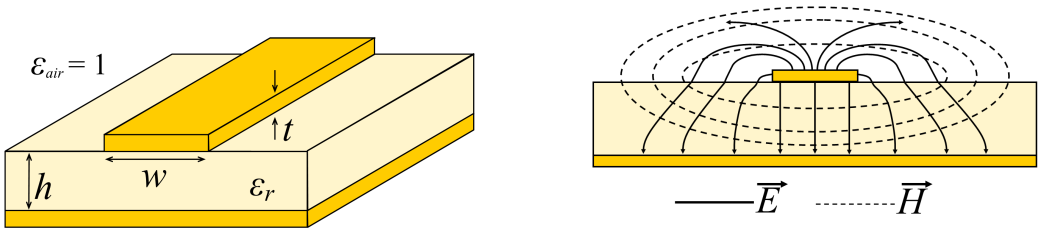

(a) (b)

Figure 2.2: Microstrip transmission line and associated fields.

Figure 2.2b illustrates the electric and magnetic fields of a microstrip line [24]. The electric and magnetic fields are partially located in the air above the dielectric substrate. Therefore, for reasons discussed in §2.1.1, microstrip lines cannot support pure TEM propagation. Instead, waves propagate in a complicated hybrid TE-TM mode. This mode is often

referred to as a *quasi-TEM* mode because the field distribution closely resembles that of a TEM wave. In fact, instead of using the exact field distribution to calculate microstrip line parameters, the calculations are greatly simplified by treating the fields as a single TEM mode in what is called the *quasi-static* approximation[3]. The expressions for line parameters below were derived by Hammerstad using the quasi-static approach [25].

In a microstrip line, waves have different phase velocities in the substrate and in the air. The quasi-static approximation treats the wave as having a single phase velocity, which is given as

$$v_p = \frac{c}{\sqrt{\epsilon_{eff}}}, \tag{2.12}$$

and the propagation constant, β, from Eq. (2.7), is given by

$$\beta = \frac{2\pi\sqrt{\epsilon_{eff}}}{\lambda_0}, \tag{2.13}$$

and the effective wavelength, λ_{eff}, is

$$\lambda_{eff} = \frac{\lambda_0}{\sqrt{\epsilon_{eff}}} = \frac{c}{f\sqrt{\epsilon_{eff}}}, \tag{2.14}$$

where c is the speed of light in vacuum, λ_0 is the free space wavelength of the microwave signal, and ϵ_{eff} is the real part of the effective permittivity assigned to the microstrip line. The effective permittivity ϵ_{eff} depends on the geometry of the line and on the relative permittivity, ϵ_r, of the substrate. It is given by

$$\epsilon_{eff} = \begin{cases} \frac{\epsilon_r+1}{2} + \frac{\epsilon_r-1}{2}\left[\frac{1}{\sqrt{1+12h/w}}\right], & \text{if } w/h \geq 1, \\ \frac{\epsilon_r+1}{2} + \frac{\epsilon_r-1}{2}\left[\frac{1}{\sqrt{1+12h/w}} + 0.04(1-w/h)^2\right], & w/h \leq 1, \end{cases} \tag{2.15}$$

where w is the width of the trace and h is the height of the substrate, as shown in Figure

[3]It is called the quasi-*static* approximation because the spatial dependence of TEM fields in a transmission line is identical to that of static fields

2.2a. This equation, in combination with Eq. (2.14), allows the frequency of a microstrip resonator to be estimated, as is discussed in §2.3.1.

With Eq. (2.15), estimates of the attenuation coefficient α can be made, and Eq. (2.13) can be used to determine β to then estimate the propagation constant γ. The main forms of loss in a microstrip line are dielectric loss and conductive loss, which can each be represented by individual attenuation coefficients α_d and α_c, respectively. The total attenuation coefficient is then $\alpha = \alpha_d + \alpha_c$, with

$$\alpha_d = \frac{\pi\epsilon_r(\epsilon_{eff}-1)\tan\frac{\epsilon''}{\epsilon'}}{\lambda_0\sqrt{\epsilon_{eff}}(\epsilon_r-1)} \qquad \text{Np/m}, \tag{2.16a}$$

$$\alpha_c = \frac{R_s}{Z_0 w} \qquad \text{Np/m}, \tag{2.16b}$$

where ϵ''/ϵ' is the loss tangent of the dielectric, λ_0 is the free space wavelength of the microwave, R_s is the surface resistivity of the conductor, Z_0 is the characteristic impedance of the line, in ohms, and the end result for α is in units of nepers per meter (Np/m). Typically, conductive losses will be greater than dielectric losses, but that depends on the specific choice of conductor and substrate. Radiation is also a significant form of loss, but it occurs mainly at discontinuities such as bends and stepped changes in trace width.

The characteristic impedance, Z_0, of microstrip lines can also be estimated using the quasi-static approach using the empirical formula

$$Z_0 = \begin{cases} \frac{120\pi/\sqrt{\epsilon_{eff}}}{[w/d+1.393+0.667\ln(w/d+1.444)]}, & \text{if } w/h > 1, \\ \frac{60}{\sqrt{\epsilon_{eff}}}\ln\left[\frac{8h}{w}+\frac{w}{4h}\right], & w/h < 1. \end{cases} \tag{2.17}$$

This formula for Z_0 facilitates the design of microstrip transmission lines that must be impedance-matched to lines and devices. Equations (2.15) and (2.17) have been shown to have relative errors of less than 1% when w/h is between 0.1 and 10 and when the frequency is between 1 GHz and 10 GHz [25]. In the work presented in this thesis, Eqs. (2.14) and

(2.15) were used to estimate microstrip resonator frequencies (§2.3.1) and Eq. (2.17) was used to design the lines that would couple to the resonators to allow for measurement of S-parameters, which are discussed in the next subsection.

2.2 Scattering Parameters

In this thesis, the behaviour of microwave devices is represented using *scattering parameters*, commonly referred to as *S-parameters*. The S-parameters are the elements of the *scattering matrix* (*S-matrix*), which completely describes the transmission and reflection of microwaves with respect to the microwaves incident at the ports of a microwave network. In this section, Chapter 4, Section 3 of *Microwave Engineering* by David M. Pozar is followed to review S-parameter theory [24], and more information can be found at references 26, 27, 28, and 29.

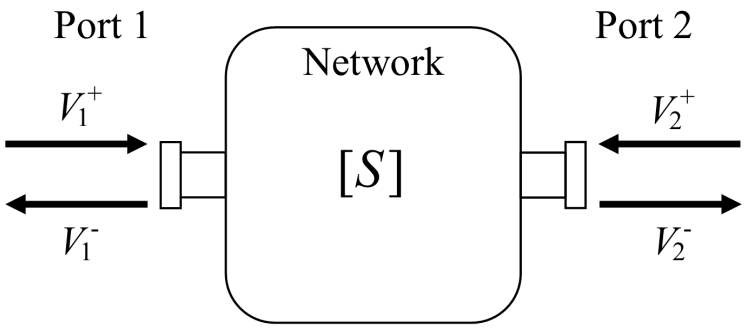

Figure 2.3: The scattering matrix describes the response of a microwave network to microwaves incident on its ports.

Consider the 2-port network shown in Figure 2.3. The amplitude of the voltage wave incident on port 1 is V_1^+ and V_1^- is the amplitude of the voltage wave originating from port 1. The same notation holds for the voltage waves at port 2. The relation between these amplitudes will depend on the properties of the network – how microwaves are transmitted

and reflected through it. The voltage wave amplitudes are linked by the S-matrix by

$$\begin{bmatrix} V_1^- \\ V_2^- \end{bmatrix} = \begin{bmatrix} S_{11} & S_{12} \\ S_{21} & S_{22} \end{bmatrix} \begin{bmatrix} V_1^+ \\ V_2^+ \end{bmatrix}, \tag{2.18}$$

or

$$[V^-] = [S][V^+].$$

The network shown in Figure 2.3 has only two ports, therefore it is described by a 2×2 matrix. In general, an N-port network will be described by an $N \times N$ S-matrix.

From Eq. (2.18) we see that the S-parameters are the reflection and transmission coefficients of the network seen at its two ports. For example, the amplitude V_2^- is obtained from Eq. (2.18) as

$$V_2^- = S_{21}V_1^+ + S_{22}V_2^+.$$

In words, the amplitude V_2^- results from the superposition of the wave transmitted from port 1 to port 2, which has an amplitude $S_{21}V_1^+$, and the wave reflected from port 2, which has an amplitude $S_{22}V_2^+$. Then, when there are no waves incident on port 2 ($V_2^+ = 0$), the transmission coefficient from port 1 to port 2 is given by $T_{21} = \frac{V_2^-}{V_1^+} = S_{21}$. Similarly, when there are no waves incident on port 1 ($V_1^+ = 0$), the reflection coefficient at port 2 is given by $\Gamma_2 = \frac{V_2^-}{V_2^+} = S_{22}$. In general, the element S_{mn} is given by

$$S_{mn} = \left.\frac{V_m^-}{V_n^+}\right|_{V_l^+=0; l\neq n}, \tag{2.19}$$

where V_l^+ represents the voltages incident on each of the ports that are not port n. Note here that the voltage amplitudes are complex quantities because they describe both the magnitude and phase of the waves. Therefore S_{mn} is also a complex value with an associated magnitude and phase. This is discussed later in this section.

The most common and useful tool used to measure S-parameters is the vector network

analyzer (VNA)[26, 27, 28, 29]. The VNA is able to generate microwaves with a precisely controlled amplitude to drive a device and accurately measure the response. To measure S_{mn}, the VNA drives the network port n with a wave of known amplitude V_n^+ and measures V_m^-, the voltage of the wave coming from port m. At the same time, the voltage of the waves incident on port m must be zero, so the VNA is designed to receive all microwaves coming from port m without reflection. Reflections of waves to other ports not under test are also eliminated by terminating the ports with matched loads. Then, S_{mn} is determined from Eq. (2.19).

As previously mentioned, microwaves undergo changes in both amplitude and phase when interacting with microwave networks. To describe both these effects, S-parameters are defined as complex values; that is, they have real and imaginary components. Expressed in exponential form, S_{mn} is given by

$$S_{mn} = |S_{mn}|e^{j\phi}, \tag{2.20}$$

where $|S_{mn}|$ is the magnitude of S_{mn}, j $(= \sqrt{-1})$ is the imaginary unit, and ϕ is the phase angle of S_{mn}. $|S_{mn}|$ is obtained from the ratio of the voltage magnitudes:

$$|S_{mn}| = \frac{|V_m^-|}{|V_n^+|}. \tag{2.21}$$

The phase ϕ is obtained from the phase difference between the input and output waves:

$$\phi = \angle V_m^- - \angle V_n^+. \tag{2.22}$$

One of the simplest networks to measure with a VNA is a single transmission line. Transmission lines are considered 2-port networks and are generally reciprocal; that is, signals propagate identically regardless of their direction ($S_{21} = S_{12}$). From S_{21}, the propagation constant, γ, (see §2.1.1) of a line of length ℓ can be determined: the magnitude gives the attenuation coefficient of the line, with $|S_{21}| = e^{-\alpha\ell}$ and the phase angle gives the phase

coefficient of the line, with $\phi = \beta\ell$ (modulo 2π).

Equation (2.21) provides the voltage gain or loss of a network. The power gain or loss of the network is obtained by squaring Eq. (2.21), as the power amplitude $|P| \propto |V|^2$. Therefore, in the example shown in Figure 2.3, a value of $|S_{21}| < 1$ corresponds to transmission loss between ports 1 and 2; a value of $|S_{21}| > 1$ corresponds to transmission gain, which indicates that the device must have an external source of power. Similarly, $|S_{11}|^2$ corresponds to the reflection power loss/gain at port 1. The same is true of $|S_{12}|^2$ and $|S_{22}|^2$ when considering waves incident on port 2.

It is sometimes convenient to express $|S_{mn}|$ on a decibel (logarithmic) scale. In such cases, it is the convention to take the ratio power amplitudes of the input and power waves. That is, the decibel value of $|S_{mn}|$ is given by

$$|S_{mn}|(dB) = 10\log_{10}\frac{|P_m^-|}{|P_n^+|} = 20\log_{10}\frac{|V_m^-|}{|V_n^+|}. \tag{2.23}$$

Typically, a VNA will have the option of presenting S-parameters in either decibel or linear units. When the decibel scale is selected, the measurement provided will correspond to Eq. (2.23); when the linear scale is selected, the measurement will correspond to Eq. (2.21)

2.3 Microstrip Resonators

2.3.1 General Theory

A resonator can be constructed from a length of microstrip transmission line by terminating both ends of it with open ends or short-circuits. Such terminations act as reflective boundaries and allow standing waves to form along the line. This section focusses on open-ended resonators, as these are the type used in the work presented later.

Standing wave modes occur in a transmission line resonator when the length of the line

is equal to an integer multiple of half-wavelengths. That is

$$\ell = n\frac{\lambda}{2} \quad ; \quad \lambda = \frac{2\ell}{n} \qquad \text{with } n = 1,2,3 \ldots, \tag{2.24}$$

where ℓ is the length of the resonator and λ is the wavelength in the transmission line. For the fundamental mode ($n = 1$), the length $\ell = \lambda/2$; for this reason, these resonators are called *half-wave* or $\lambda/2$ resonators.

As stated in §2.1.2, signals propagate along microstrip transmission line with an effective wavelength, λ_{eff}, given by Eq. (2.14). Combining the expression for λ_{eff} with Eq. (2.24), the fundamental frequency, f_0, of a microstrip resonator is given by

$$f_0 = \frac{c}{2\ell\sqrt{\epsilon_{eff}}}. \tag{2.25}$$

The above equation can be used, along with Eqs. (2.15) and (2.17), to design a microstrip resonator with a desired frequency.

The value of the resonant frequency will also be affected by the structure of the resonator, such as loops, corners, and changes in trace width. These effects are difficult to determine analytically, and it is generally simpler to use Eq. (2.25) to design a resonator with the desired frequency using CAD and simulation software and adjust the design to bring the resonant frequency to the desired value.

At frequencies near resonance, the open-ended microstrip resonator can be modelled as a lumped-element parallel RLC circuit, as shown in Figure 2.4.

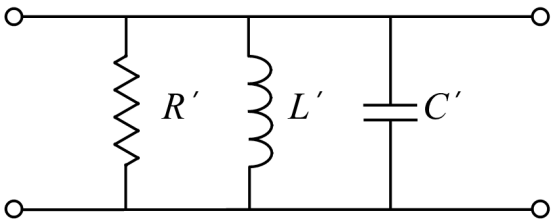

Figure 2.4: For frequencies near resonance, an open-ended half-wave microstrip resonator can be modelled as a parallel RLC circuit.

Here, power dissipation is represented by the resistance R', and the storage of magnetic energy and electric energy are represented by the inductance L' and capacitance C', respectively. These lumped-element equivalent parameters are related to, but distinct from, the distributed parameters L, C, R, and G described in §2.1.1.

The resonant frequency, f_0, can be defined in terms of the equivalent parameters as

$$f_0 = \frac{1}{2\pi\sqrt{L'C'}}. \tag{2.26}$$

Another parameter of interest is the input impedance, Z_{in}, of the resonator. It is given by

$$Z_{in} = \left(\frac{1}{R'} + \frac{1}{j\omega L'} + j\omega C'\right)^{-1}, \tag{2.27}$$

where $\omega = 2\pi f$ is the angular frequency of the input microwave. At resonance, $\omega = 1/\sqrt{L'C'}$ and $Z_{in} = R'$.

An important figure of merit for resonators is the *quality factor* (*Q-factor*). It provides a measure of the ability of the resonator to store energy. Generally, the Q-factor is defined as

$$Q = \omega \frac{\text{average energy stored}}{\text{energy dissipated per cycle}}. \tag{2.28}$$

Therefore, a higher Q-factor corresponds to a lower damping in the resonator, and a lower Q-factor corresponds to a higher damping. The broad definition listed above manifests itself differently according to the type of resonator being considered, but another general and more easily quantifiable definition of the Q-factor is

$$Q = \frac{\omega_0}{\Delta\omega} = \frac{f_0}{\Delta f}, \tag{2.29}$$

where Δf is the full-width-at-half maximum of the resonance peak when measured as e.g.

S_{21}. From Eq. (2.28) and (2.29)we see that a high-Q (low-loss) resonator will have a sharp resonance peak; this fact is critical to the operation of the devices used in the work presented in chapters 3 and 4.

In an open-ended half-wave microstrip resonator, the Q-factor is given by

$$Q = \omega_0 R' C' = \frac{R'}{\omega_0 L'}, \tag{2.30}$$

which can also be expressed in terms of the phase-change coefficient, β and the attenuation coefficient, α, (see §2.1.1) of the transmission line as

$$Q = \frac{\beta}{2\alpha} \tag{2.31}$$

The Q-factor can also be decomposed according to the different forms of loss in a resonator. In a microstrip resonator, there are three main forms of loss: dielectric loss (denoted by Q_d), conductor loss (Q_c), and radiation loss (Q_r). Together, they represent the total loss and overall Q, with

$$\frac{1}{Q} = \frac{1}{Q_d} + \frac{1}{Q_c} + \frac{1}{Q_r}. \tag{2.32}$$

Similarly, coupling the resonator to an external system will introduce additional energy loss, which can also be represented by an external Q-factor, Q_{ext}. When a resonator is coupled to an external resonator, it is said to be *loaded*, and the resonator will have an unloaded Q-factor Q_u and a loaded Q-factor, Q_L, with the latter given by

$$\frac{1}{Q_L} = \frac{1}{Q_u} + \frac{1}{Q_{ext}}. \tag{2.33}$$

In general, Q_{ext} will depend on the particularities of the external system and the type of coupling.

Microstrip resonators, in general, have Q-factors on the order of 10^2. As implied from

Eq. (2.32), the exact Q-factor depends on dielectric loss in the substrate, resistive losses in the conductor, and radiation losses stemming from the resonator geometry.

2.3.2 Sensing with Microstrip Resonators

Microstrip resonators are suited to many sensing applications. The electromagnetic fields of the resonator can be used to probe an object of interest because their situation in the open air makes them accessible for measurements. With Eqs. (2.1) through (2.6), it is seen that the propagation characteristics of transmission line depends on the material in which the fields are located. In §2.3.1, it was shown that the resonance peak width and frequency of microstrip resonators depends on the propagation characteristics of the constituting transmission line. Therefore, measurements are made from changes in the frequency response of the resonator caused when objects are placed in its fields, or when objects already in the fields undergo changes that affect its permittivity or permeability. Microstrip resonators have been used in this way to, for example, measure the complex permittivity of materials [30], to detect single cell movement [18] and to assess yeast cell viability [31].

Since the performance of a microstrip resonator-based sensor depends on its ability to resolve shifts in the resonance peak, a high Q-factor, which is associated with a narrower resonance peak, is desirable. The following section describes how the resolution of a resonator-based sensor is improved by the inclusion of an active component that compensates for energy loss in the resonator.

2.3.3 Active Resonators

The term "active resonator" refers to a resonator in which an active element has been included to counteract energy loss in the resonator. As per Eqs. (2.28) and (2.29), the decrease in loss creates a drastically narrower resonance. In principle, a fully loss-compensated resonator has an infinite Q-factor (the denominator in Eq. (2.28) is zero). In practice, microstrip resonators with Q-factors on the order of 10^4 have been achieved [32]. This value compares

to the Q-factors on the order of 10^2 of passive resonators (i.e. resonators lacking an active element). Thus, smaller resonance shifts can be discerned when using active resonators as sensors, allowing more sensitive measurements to be made with active resonators than with their passive counterparts. Active resonators are the central component in the sensors presented in Chapters 3 and 4.

The active resonators first developed and fabricated by our group consisted of a passive resonator coupled to an external active feedback circuit to compensate for loss in the resonator [17]. The active circuit was designed to supply RF power to the passive resonator with a phase such that the introduced waves interfered constructively rather than destructively with the oscillations of the passive resonator. The active component of the feedback circuit was a transistor amplifier with a gain adjusted to maintain the stability of the active resonator [19]. The conditions for stable active resonance were therefore expressed in terms of the Q-factors of the coupled feedback loop, the passive resonator, and in terms of the amplifier gain. Phase-matching conditions were also a necessary consideration.

In the process of attempting to fabricate active resonators for ourselves, our group has discovered that, for the purposes of our own research, active resonators can be constructed as a single structure without the need of an external feedback circuit. This structure consists of a single microstrip resonator with an integrated transistor amplifier, and we have achieved Q-factors on the order of 10^4 in such devices. We have been quick to explore new applications for these resonator sensors, such as in the study of magnon-photon coupling, and, of course, the work presented in this thesis.

Since the active resonators we fabricate in our lab function without an external feedback circuit, the established theoretical description of the feedback-based active resonators perhaps do not directly apply to our own devices. As a result, a complete theoretical description of our active resonators has not yet been developed. However, we have observed that our active resonators produce an RF output when only DC power is supplied to it, which invites the treatment of the active resonators as oscillators when attempting to describe them. Be-

low is offered a theoretical description of the active resonators based on the descriptions of transistor oscillators provided by Pozar [24].

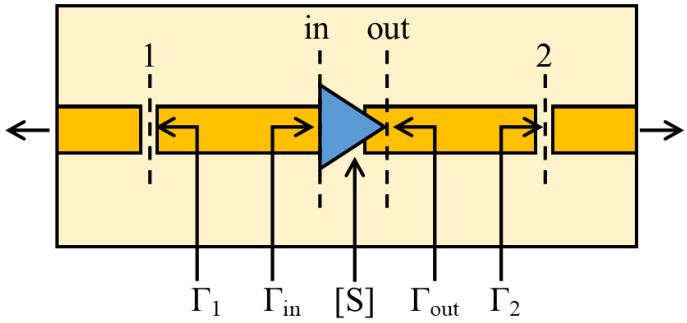

Figure 2.5: An oscillator can be constructed using a transistor amplifier embedded in a microstrip resonator. Feed lines are coupled with gaps 1 and 2, and reflection occurs at these boundaries with respective reflection coefficients Γ. The reflection coefficients Γ_{in} and Γ_{out} account for the total reflection from subsequent boundaries and not just the reflections at the *in* and *out* boundaries of the amplifier.

The active resonators constructed in our lab consist of a transistor amplifier embedded in the centre of a microstrip resonator, as is shown diagrammatically in Figure 2.5. The resonator is gap-coupled to feed lines, which in turn can be connected to a VNA or other apparatus. To explain the conditions for stable oscillation, we consider four reflection boundaries: the reflections at the coupling gaps, with reflection coefficients Γ_1 and Γ_2, and the reflections as seen from the input and output of the amplifier, with reflection coefficients Γ_{in} and Γ_{out}. The reflection coefficient Γ_{in} is affected not only by the waves reflected at the input boundary of the amplifier, but also those that have transmitted and reflected from gap 2. Taking this fact into consideration, the input reflection coefficient is given by

$$\Gamma_{in} = S_{11} + \frac{S_{12}S_{21}\Gamma_2}{1 - S_{22}\Gamma_2} = \frac{S_{11} - \Delta\Gamma_2}{1 - S_{22}\Gamma_2}, \tag{2.34}$$

where Δ is the determinant of the S-matrix describing the amplifier, which is given by

$$\Delta = S_{11}S_{22} - S_{12}S_{21}. \tag{2.35}$$

For stable oscillations to occur at the output of the amplifier, the net energy loss at the input of the amplifier must be zero. Since waves are reflecting between gap 1 and gap 2, this condition is expressed mathematically as $\Gamma_{in}\Gamma_1 = 1$, remembering that Γ_{in} takes into account waves that have been amplified and reflected backwards through the amplifier. Since energy is lost at gap 1, $\Gamma_1 < 1$, and we must have $\Gamma_{in} > 1$ for stable oscillation. Since Γ_{in} depends strongly on the the characteristics of the amplifier, a necessary condition for oscillation can be defined in terms of the amplifier S-parameters. This condition is

$$K = \frac{1 + |\Delta|^2 - |S_{11}|^2 - |S_{22}|^2}{2|S_{12}S_{21}|} < 1. \tag{2.36}$$

This test is essentially the reverse of Rollet's condition for unconditional stability in microwave transistor amplifiers [24]. If the inequality in Eq. (2.36) is not true, then it is impossible for oscillations to occur for the given amplifier at the frequency in question.

The description above offers some insight into the operation of our active resonators, but a complete theoretical description is still under development. In practice, to fabricate active resonators we use CAD software to design and simulate active resonators for a desired frequency.

3

Detection of External Insects

3.1 Introduction

External insect pests are insects that live in between grain kernels as opposed to inside them. They are free to move throughout the grain bulk, so one method of detecting and monitoring them is by using traps [2]. Other common methods involve pulling a sample from the bulk and separating the insects from the grain such as by shaking and sieving the grain or by using a Berlese funnel, as discussed in Chapter 1. The detection of external insects has also been achieved in storage bins using acoustical methods [33]. External insects' freedom of movement in grain also makes possible the use of Doppler microwave radar to detect insects in grain samples [6]. However, microwave radar has not yet been shown to be useful in storage bins.

In this chapter, a demonstration of novel microwave sensors for the monitoring of stored product pest insects is presented. The sensing element of the device is a planar active microwave resonator, as described in §2.3.3. It is constructed from microstrip and has a Q factor as high as 21,600 even in lossy environments, which is a factor 900 greater than the conventional passive resonator (Q = 24) in the same environment. Insect detection is achieved when insects move within the electric field of the resonator, causing changes to the

propagation characteristics of the microstrip resonator, as described in §2.1.1. The high Q factor of the resonator results in a very narrow resonance, allowing the small shifts in the resonance frequency caused by insect movement to be resolved.

The demonstration was performed stepwise. First, we confirmed that insects indeed trigger a response in the sensors. Then, we showed that the sensor response was related to insect activity levels. Finally, as a proof-of-concept, we demonstrated that the sensors function when covered in grain and are able to detect insect activity in grain samples. Judging from these results, the sensor could potentially be used in grain bins to monitor for insect activity.

The results in this chapter were submitted for publication to *Biosystems Engineering* in October 2017.

3.2 Materials and Methods

3.2.1 Experimental Apparatus

In order to test the sensor, we constructed a device which integrates the sensor with the ability to confine insects, hold grain samples, and control temperature. Figure 3.1 illustrates the set-up for the experiments reported in this work. To prevent insects from escaping, a containment area was constructed on top of the resonator by fastening a 26 mm diameter, 80 mm high glass cylinder to the surface. The cylinder was closed at one end, and its open end was fixed to the resonator. To control the temperature, a Peltier cell was placed on the side of the board opposite to the resonator. The cell was supplied with a bench top power supply, and transferred heat to and from a metal optics table, which acted as a thermal reservoir and on which the board was secured. The temperature of the containment area was measured using a K-type thermocouple with a Fluke 179 digital multimeter (Everett, WA, USA).

The resonators were fabricated using microstrip technology. The planar cavities were

designed using Computer Simulation Technology (CST) Studio (Darmstadt, Germany) and constructed in-house by milling a double-sided 35 μm copper clad FR-4 substrate for the active resonator and Rogers DiClad 527 substrate[1] (Rogers, CT, USA) (which has lower dielectric loss than FR-4) [34] for the passive resonator using a LPKF ProtoMat S103 board milling machine (Garbsen, Germany). The thickness of both substrates was 1.6 mm. Each resonator was gap-coupled in series to 50 Ω transmission line. An Agilent PNA-L N5230C vector network analyser (VNA) (Santa Rosa, CA, USA) was used to measure the frequency response of the resonators. Here, the transmission coefficient was measured as S_{21}, a complex vector quantity whose magnitude, $|S_{21}|$, is equal to the ratio of the device output to input

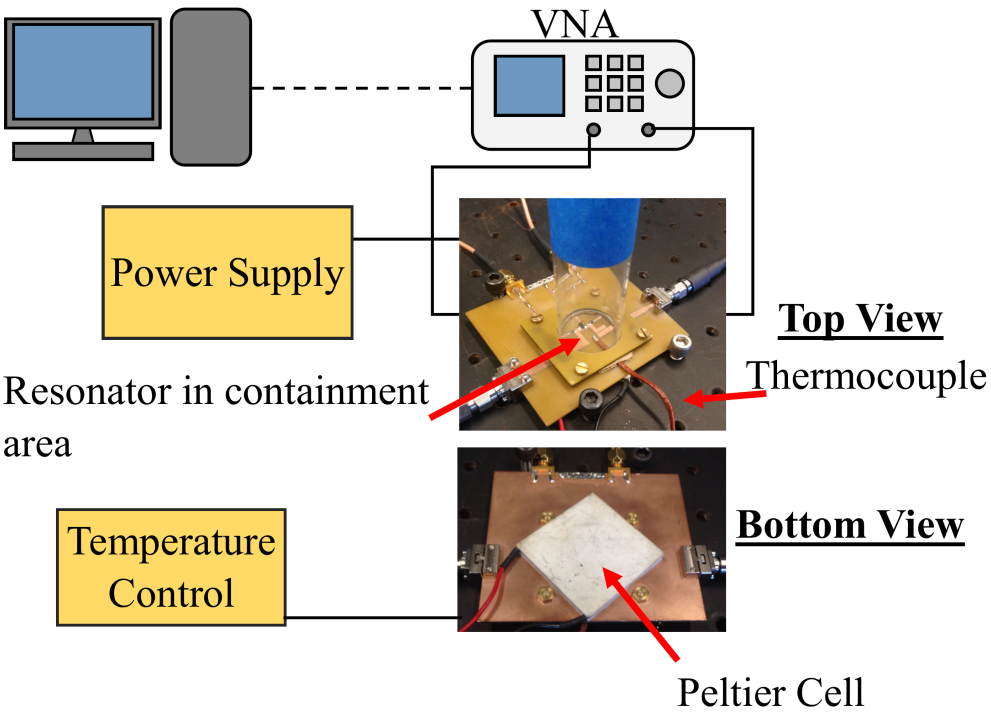

Figure 3.1: A diagram of the experimental set-up. A vector network analyser (VNA) was used to measure the transmission spectrum of the active resonator. The active resonator received external power and had a glass cylinder affixed to contain insects. On the underside of the resonator, a Peltier cell enabled heating and cooling of the resonator to control insect activity levels. The device was secured to a metal optics table top which functions as a heat sink for the Peltier cell.

[1]The designation "FR-4" refers to a grade of material defined by its mechanical, chemical, and electrical properties and is a common choice of substrate for printed circuit boards. Conversely, DiClad 527 is a specific material product offered by Rogers Corporation.

voltage wave amplitudes and is commonly expressed on either linear or logarithmic (decibel) scales. Unless specified otherwise, the output power of VNA was set to -20 dBm with -20 dB external attenuation resulting in -40 dBm (0.1 μW) power input to the sensor and an IF bandwidth (the bandwidth of the baseband IF filter internal to the VNA) setting of 1.5 kHz. For all measurements, the testing area was shielded with microwave absorber [Cumings Microwave C-RAM LF-77 (Avon, MA, USA)] to block interfering signals during measurement.

3.2.2 Insects and Grain

We tested two stored-product insects; the rusty grain beetle, *Cryptolestes ferrugineus* (Stephens) (Laemophloeidae: Coleoptera) and the red flour beetle, *Tribolium castaneum* (Herbst) (Tenebrionidae: Coleoptera). The insects were collected from a grain storage in Manitoba, Canada in 2013, and reared at 30 °C since that time. *Cryptolestes ferrugineus* was reared on Hard Red Spring wheat kernels, cracked wheat and wheat germ. *Tribolium castaneum* was reared on white flour with 5% brewers yeast. Only adult insects having emerged from pupae less than 2 months prior were used in this study.

The grain used in the grain sample tests was Hard Red Spring wheat (cv. Carberry) with a moisture content of 12.9% $\pm$ 0.1% [35].

3.2.3 Procedure for Contact Sensing Experiment

In our first experiment, we used the sensor to detect insect activity by contact. We placed a single adult on the surface of the resonator and recorded the transmission spectrum. Insect movement on the surface caused the transmission spectrum to shift (Figure 3.2). A glass cylinder (26 mm diameter, 80 mm height) was fastened to the sensor board to prevent insect escape (Figure 3.1). The containment area was at a room temperature of approximately 23 °C. To reliably detect the insect, we continuously recorded S_{21} for about 10 min, corresponding to 960 individual spectrum measurements. From the measurement, we determined the

peak transmission frequency, f_0, using a peak fitting algorithm.

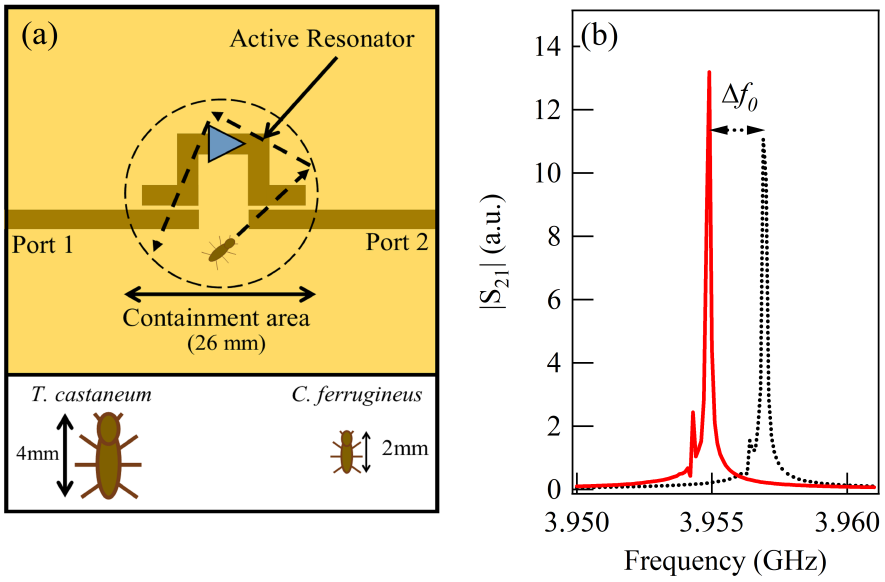

Figure 3.2: The sensor could detect insects by contact. (a) a single insect was placed on the resonator surface and was confined by a glass cylinder (26mm diameter). The measurement was repeated with two insect species: *Tribolium castaneum* and the smaller *Cryptolestes ferrugineus*. (b) Changes in insect position caused a shift of the peak transmission frequency, f_0, of the resonator.

3.2.4 Procedure for Activity Measurement

An insect was placed in the containment area and allowed to move freely on the surface of the resonator, as in Section 3.2.3. A Peltier cell placed under the board enabled heating and cooling of the resonator (Figure 3.1) depending on the polarity of the voltage bias. The temperature was controlled by adjusting the voltage supplied to the Peltier cell. Insect activity was measured for 10 temperatures ranging from 10 °C to 50 °C. For each temperature point, the containment area was left to equilibrate – a process taking approximately 10 min – before data were recorded. We then recorded the transmission spectrum over a 10 min period at a constant rate of approximately one every second, corresponding to 600 individual measurements. The measurement was repeated with 5 adult individuals from each species. The measurement area was shielded from interfering radiation.

From the recorded spectra, f_0 as it varied with time was obtained. A statistical analysis of the recorded activity was performed. To quantify the level of insect activity at a given temperature, the average of the absolute difference in f_0 between consecutive time points was calculated for that measurement. This average is labelled δf_0 in this report. Then, the overall mean across all measurements and the standard error of the mean were calculated for each temperature, for both species. In this way, the level of insect activity as it varies with temperature was estimated.

3.2.5 Procedure for Detection in a Grain Sample

An important practical application of the sensor is the detection of insects in grain samples or bulks. First, we compared the effects of the dielectric loss caused by grain when it covered a passive resonator and active resonator. This was done by gradually filling the containment area of the test device with grain until the further addition of grain did not affect the transmission spectrum of the resonator (roughly 3 cm for the active resonator). This was repeated for the passive resonator and the active resonator, and the transmission spectrum of each was recorded in the cases with and without grain.

As a proof-of-principle of detection in grain, we partially filled the 26 mm glass cylinder with wheat grain and introduced a single insect on the surface of the wheat held inside the cylinder. We then recorded the transmission spectrum every 0.6 s for 10 min. Over the course of the measurement, the insect was left free to move on and inside the wheat sample. The measurement was repeated with grain heights varying from 0.6 cm to 2.1 cm for *T. castaneum* and 0.3 cm to 1.2 cm for *C. ferrugineus*. The measurements were conducted at room temperature of approximately 23 °C and the sensor was shielded from interfering radiation.

To quantify the measured activity, we measured δf_0 in the same way described in Section 3.2.4.

3.3 Results and Discussion

3.3.1 Contact Sensing

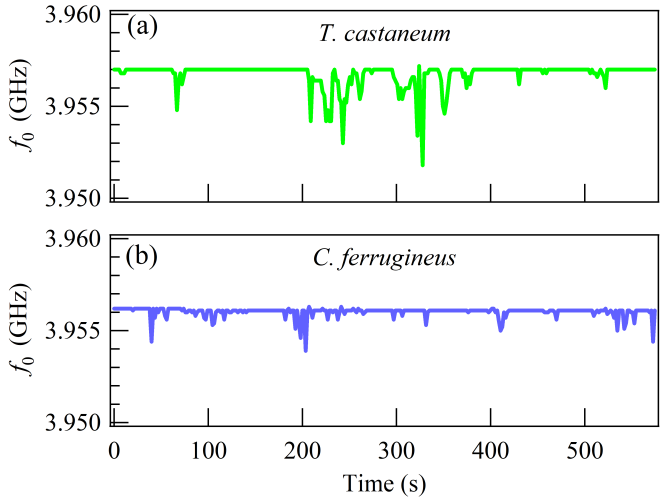

Figure 3.3: Typical measurements of the recorded peak transmission frequency, f_0, over time, for each species tested.

The frequency at which maximum transmission occurs, f_0, is plotted in Figures 3.3 (a) and (b). A clear signal was observed for both species, and the magnitude of the shifts was found to depend on the size of the insect and its trajectory through the sensitive area of the resonator. The greatest shift was observed when the insect was located in one of the two coupling gaps, because signals must transmit through these gaps to enter or exit the resonator. Unsurprisingly, the maximum shift of 5 MHz caused by the larger *T. castaneum* was greater than the 2.5 MHz shift caused by *C. ferrugineus* (half the size of *T. castaneum*). This is because *T. castaneum* occupied a greater portion of the electric field than *C. ferrugineus*, so its effect on the resonance was stronger. The fact that the resonance shifts spanned a range of values and did not simply jump between two states indicated that the transmission peak shifted gradually as the insect moved through the electric field of the resonator, whose strength was position-dependent. The maximum shifts correspond to instances when the insect was located in the region where the electric field was strongest, viz. the coupling

gaps and the edges of the resonator structure. When the insect was on the edge of the containment area (where the microwave fields were weak) no shifts are apparent. For this measurement the VNA was configured for a sufficiently large bandwidth to capture the shifts but also rapid enough to capture insect movement. With these settings, insect movement at the periphery of the glass cylinder was not apparent. However, as we show in the Section 3.3.3, it is possible to detect insect movement without direct contact to the device.

3.3.2 Activity Measurement

Insect activity depends strongly on the ambient temperature. *Tribolium castaneum* and *C. ferrugineus* movements are greatly reduced at temperatures below 10°C [36] and 8°C [37], respectively. Temperatures greater than 45 °C are fatal to both species [38]. In our second experiment, we demonstrated the ability of the sensor to monitor insect activity by performing contact measurements at different temperatures.

Figure 3.4 displays the peak transmission frequency for both species at selected temperatures spanning the range of temperatures to which insects were exposed.

Tribolium castaneum is about 2 times longer than *C. ferrugineus*, and therefore causes larger shifts, which accounts for its generally greater measured activity. In both species, the measured activity was highest between 20 and 30 °C and decreased outside this range. For both species, measured activity lowered at low temperatures, which is in agreement with the published observations that temperatures below 15 and 17.5 °C inhibit movement in *T. castaneum* [39] and *C. ferrugineus* [40], respectively. On the other hand, temperatures greater than 40 °C are uncomfortable for both species and caused them to circle the edge of the containment area in an attempt to seek cooler temperatures, explaining the relative decrease in measured activity in this temperature range. Temperatures greater than 50 °C will kill most individuals from both species after 2 hours exposure [36, 37]. Conversely, *C. ferrugineus* prefers temperatures of 30 - 36.5 °C [41] and *T. castaneum* has been observed to move along a temperature gradient to areas of 30 °C [39] suggesting a preference for

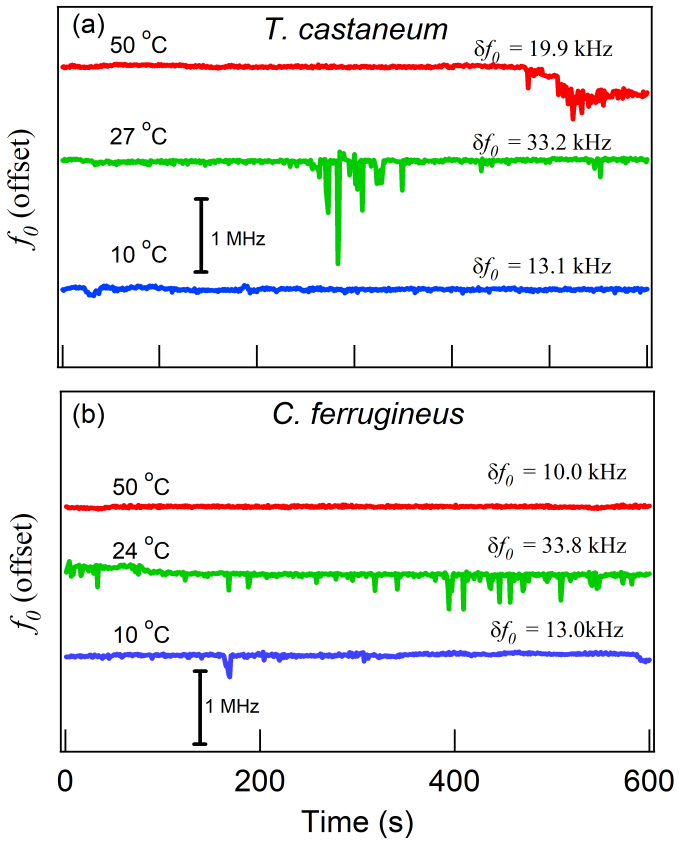

Figure 3.4: The peak transmission frequency (f_0) over 10 min measurement periods when a single insect was placed in the containment area for different temperatures. The average absolute peak shift between consecutive spectrum measurements (δf_0) was used as a measure of the activity. The spectrum was recorded approximately every second for 10 min.

similar temperatures, and so activity measured in this temperature range was markedly lower. Activity was highest from 20 to 30°C because the temperature was not so low as to inhibit movement, not too comfortable as to discourage movement, and not so high as to incite escape.

3.3.3 Detection in Grain Samples

The grain increases the difficulty of insect detection through several factors: 1) insect movement is restricted to the pore spaces between kernels; 2) the contrast between the dielectric constant of the insect and the grain environment is lower compared to that with an air environment, so the response of the sensor to the insect may be weaker; 3) grain introduces

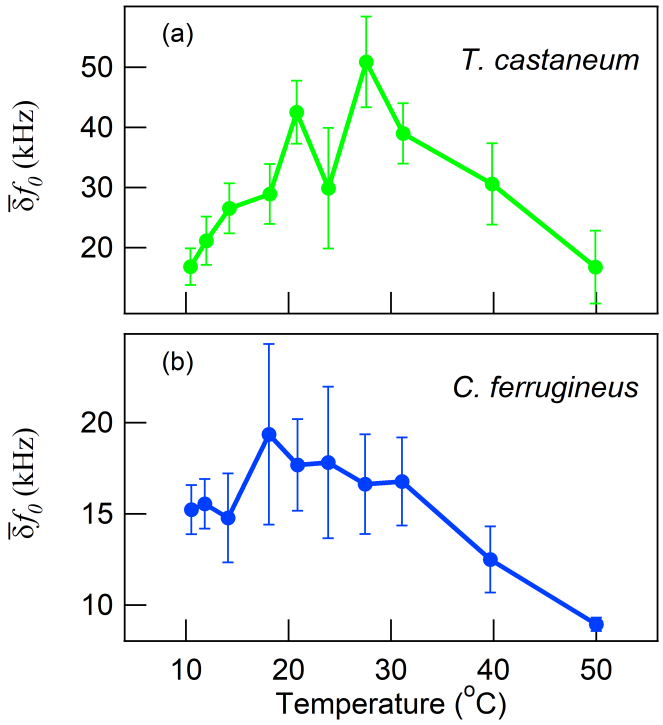

Figure 3.5: The measured activity of both species as it varied with the temperature of the containment area. The points shown are averages across 5 repetitions, each with different individuals, for each species. Verticals error bars represent the standard error of the mean.

dielectric loss and increases the resonance width, which decreases the sensor's ability to resolve resonance shifts. Of these factors, we expected the first and last to be most important. Peak broadening was mitigated by using an active resonator, which experiences minimal peak broadening against loss and thus could detect the movement of insects in grain samples.

As a demonstration of the effects of grain on the transmission spectrum of the resonator, we covered with wheat grain a passive resonator and compared the result to when we did the same to the active resonator. The results are shown in Figure 3.6. The construction of the passive resonator is described in Section 3.2.1. The effect of the increased dielectric absorption was significant in the passive resonator, whose resonance width increased by over 350% [Figure 3.6 (a)]. Conversely, the active resonator experienced an increase in resonance width of only roughly 20% while maintaining a very sharp transmission peak [Figure 3.6 (b)]. As we show below, the resistance of the active resonator to increased dielectric loss was

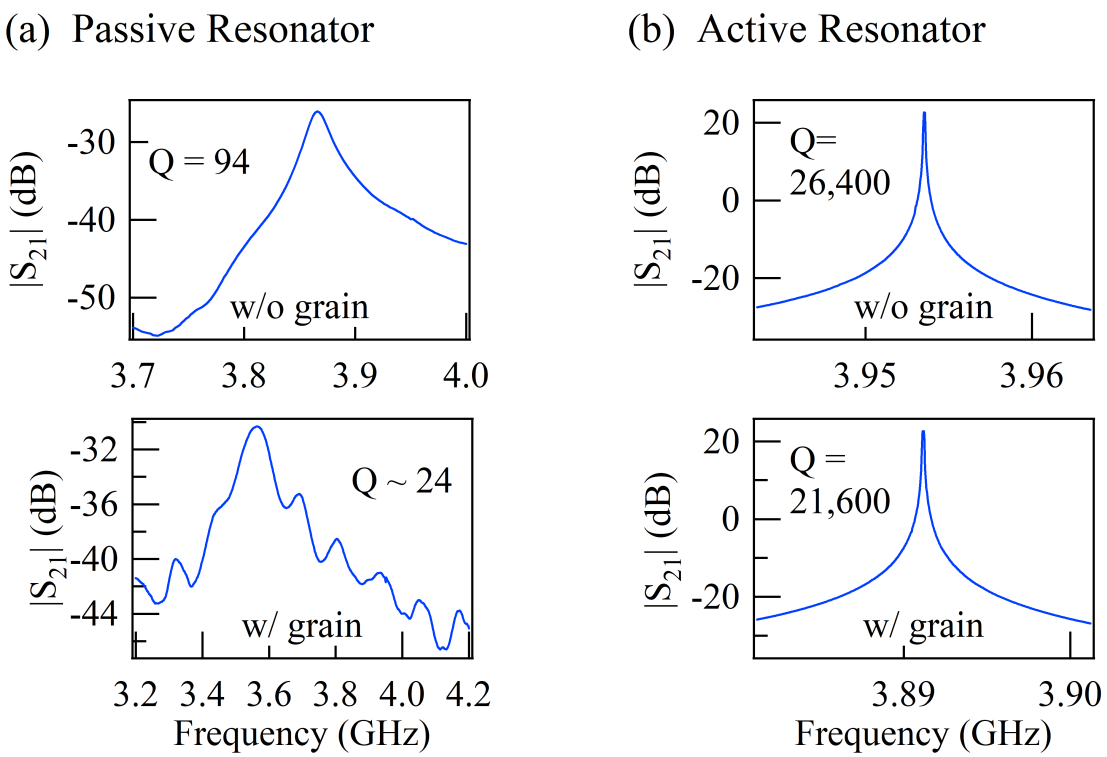

Figure 3.6: (a) the transmission spectrum, $|S_{21}|$ as a function of the microwave frequency, of an air-loaded (no grain) and grain-loaded passive resonator. (b) $|S_{21}|$ of an air-loaded and grain-loaded active resonator. Note the difference in horizontal scales between the two resonators. Loading the resonator with grain also caused a shift in the transmission peak. $|S_{21}|$ is depicted on a dB scale.

crucial to its ability to detect insects in grain.

Figure 3.7 shows the response of the sensor to single insects in grain samples of various sizes. Using the case without insects [Figure 3.7 (b)] as a reference, we saw an indication of activity for *T. castaneum* in Figure 3.7 (c) and *C. ferrugineus* in Figure 3.7 (d), which had manifested as a signal with seemingly random variations as well as temporary deviations of noticeably greater amplitude. These features might reflect two scales of motion: the random short scale motion of the insect as it searched for paths between individual grains and the longer scale motion as it moved through the sample.

The results highlight the necessity of the active resonator. The shifts caused by the insect in grain were dramatically smaller when compared to those from contact, decreasing from a few megahertz to at most tens of kilohertz. The greatest variations in f_0 seen in Figure

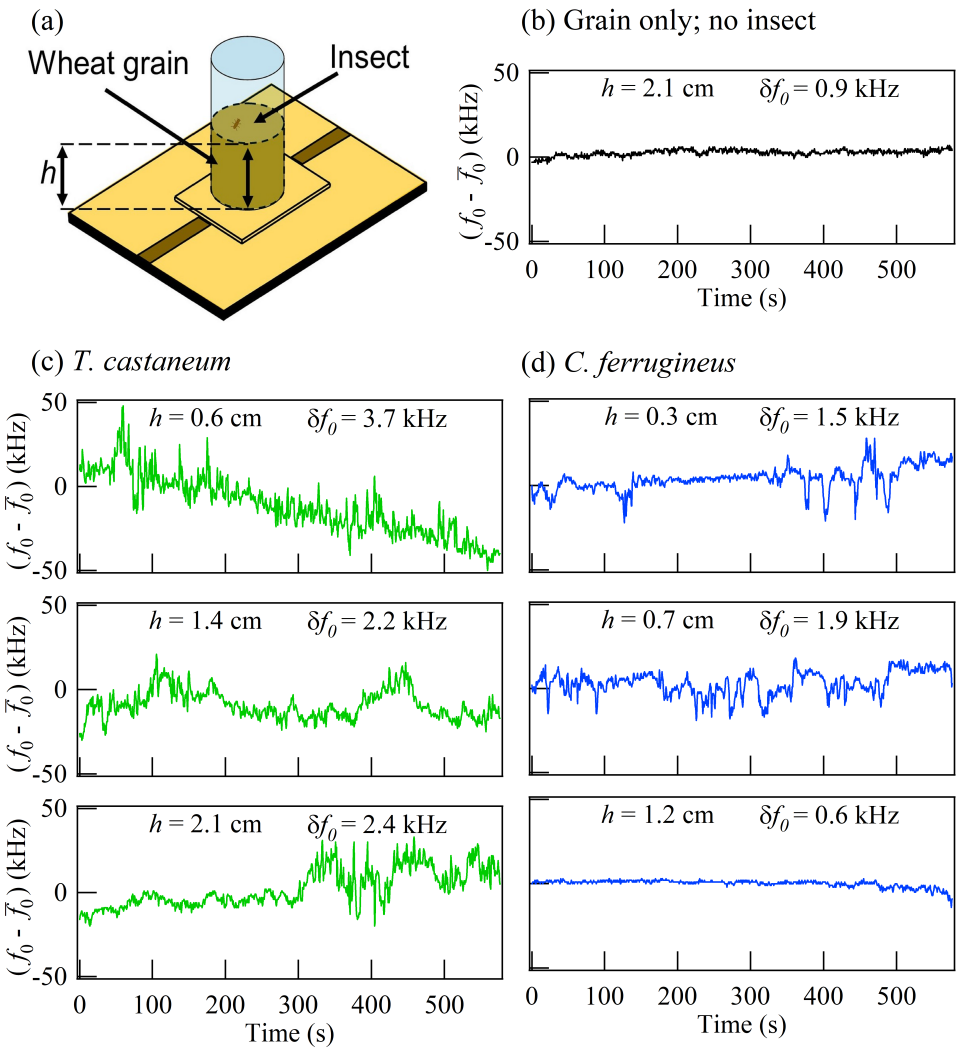

Figure 3.7: The peak transmission frequency, f_0, over time when the containment area was filled with grain of height h. (a) a diagram of the set-up. (b) f_0 over time when grain without insects was placed in the containment area. The values presented are adjusted by the subtracting the average of f_0 for the measurement, $\bar{f}_0$, from all points. (c) a single *T. castaneum* insect in 0.6 cm, 1.4 cm and 2.1 cm of grain, respectively; (d) a single *C. ferrugineus* insect in 0.3 cm, 0.7 cm, and 1.2 cm of grain. The average absolute peak shift between consecutive spectrum measurements (δf_0) was used as a measure of the activity. Each measurement was performed over a 10 min duration with the transmission spectrum recorded every 0.6 s.

3.7 span approximately 50 kHz, corresponding to 28% of the active resonator linewidth, but only 0.03% of the passive resonator linewidth when in grain [Figure 3.6]. Considering that most of the variations observed in Figure 3.7 were much smaller than 50 kHz and noting the width of the resonance of the passive resonator [Figure 3.6 (a)], we concluded that without

the active element, a passive microstrip resonator lacked the resolution to be useful for the detection of insects in grain samples.

Due to its size, *T. castaneum* movement in the grain was restricted and a net displacement from the surface where it was introduced was difficult for it to achieve [39]. This restriction may be apparent in Figures 3.7 (c) and (d), where temporary changes in f_0 were observed when the insect attempted to move deeper into the grain sample but failed to find a path leading deeper and so returned to the surface and caused f_0 to return nearly to its initial value. Figures 3.7 (c) and (d) also show constant smaller, more rapid variations in f_0 not observed in the clean case [Figure 3.7 (b)]. As the height of the sample was increased, these variations were diminished by the generally increasing distance of the insect from the resonator.

Similar features were observed in the measurement of *C. ferrugineus* movement in the grain. Since *C. ferrugineus* is significantly smaller than *T. castaneum* and was able to move more freely through the interstices of the sample, the relatively large changes in f_0 were more frequent than those observed with *T. castaneum*. However, the smaller size also reduced overall magnitude of shifts in f_0, making it more difficult to detect *C. ferrugineus* at larger distances.

3.4 Conclusions

3.4.1 Summary

We have demonstrated that the sensor based on a planar microwave active cavity was capable of detecting single adult insect activity through contact as well as in grain samples. Insect activity was detected by monitoring the transmission spectrum of the cavity, which operated in the 3-4 GHz range and whose peak transmission shifted when insects were nearby. In contrast with a passive cavity, the active cavity had a very narrow transmission spectrum peak, allowing shifts on the order of kHz to be detected. Furthermore, the active cavity

was resistant to added dielectric loss in the environment such that it maintained its narrow transmission peak even when placed in grain. We used two species of common grain pests as subjects in our tests: *T. castaneum* and *C. ferrugineus*. As expected, the larger *T. castaneum* caused greater shifts in the transmission peak than the smaller *C. ferrugineus*. This size difference resulted in a lower measured activity of *C. ferrugineus*, so the lower level of measured activity did not necessarily represent a lower level of movement. We also successfully detected the insects in wheat grain samples at distances up to 2.1 cm with *T. castaneum* and 1.2 cm with *C. ferrugineus*. Our approach has potential use as a tool to monitor insect populations in stored grain bulks, such as grain bins, or to non-destructively detect other pests such as termites

3.4.2 Future Work

Since the sensor response changes with insect activity, it has the potential for use in monitoring insect population densities in stored grain. Such monitoring is crucial for farmers and grain handlers who depend on the information to formulate their pest management strategies. A current challenge of this application is the possible ambiguities in sensor signal that results from the dependence of the response on insect size, location, and movement speed. One way to circumvent this limitation is the use of an array of sensors sunk into grain bulks to increase the reliability of detection. For example, if the sensors in an array are monitored using individual channels, the signals received on different channels can be correlated and their amplitudes compared to estimate the location of the insects producing the signal.

The sensor could also be used to quickly test for insects in grain samples pulled from a grain bulk. The usefulness of such tests would be greatly improved if insects inside kernels were also detected. In the following chapter, it is shown that the sensor can in fact make such detections.

.

4

Detection of Internal Insects

4.1 Introduction

In this chapter, the work we performed to demonstrate the active resonator sensor's capability to detect live insects hidden inside kernels of wheat is presented. Internal insect infestations are a serious concern to farmers and grain handlers because they are difficult to detect. Because internal insects are difficult or impossible to separate from the grain, they are generally undetectable by methods used for detecting external insects. Furthermore, infested kernels are difficult to identify because they bear few differences from sound kernels when examined visually. Consequently, infestations can be carried from one facility to another without being noticed, where they could reduce grain store quality and quantity. For this reason, several techniques have been developed to detect internal insects. Examples of techniques demonstrated to detect internal insects are acoustic detection, electrical conductance, nuclear magnetic resonance (NMR) spectroscopy, kernel staining, flotation, near infra-red reflectance (NIR) spectroscopy, and x-ray imaging. A brief description of each of the above techniques was given in Chapter 1.

4.2 Methods

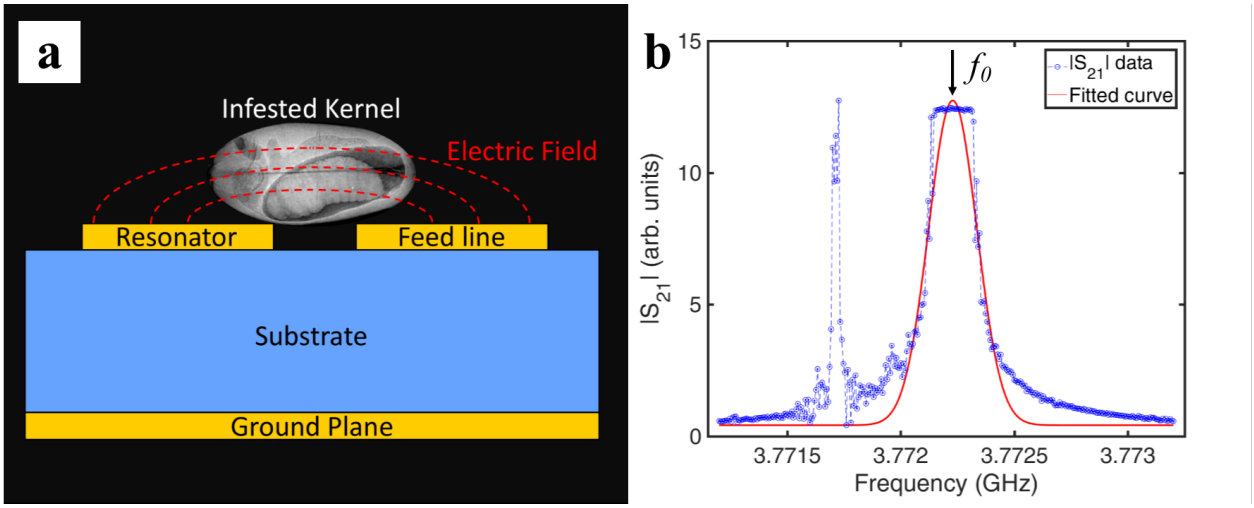

Figure 4.1: (a) A diagram of the cross-section of the resonator. Feed lines transmit power to the resonator via capacitive coupling. Kernels placed on the surface of the planar resonator are probed by electric fields. (b) The transmission spectrum of the resonator. The transmission peak centre, f_0, was obtained by fitting a Gaussian curve. Movements of insects through the electric fields cause the spectrum to shift..

4.2.1 Activity monitoring

The presented in this chapter consists of a planar microwave resonator through which the transmission of signals is greatest near the resonance frequency (Figure 4.1b). Microwave frequency electric fields extend into nearby space as they propagate along the feed line and resonator (Figure 4.1a). Perturbations of the fields, such as the introduction of an object, cause the resonance to shift to a different frequency. With this principle, the movement of insects inside kernels can be detected by probing the kernels with the electric fields and monitoring the transmission of microwaves through the resonator (Figure 4.1a).

Our measurements consisted of placing an infested kernel on the sensor and monitoring a bandwidth of the transmission spectrum containing the resonance to capture the shifts in the resonance caused by insect movement. We used a vector network analyzer (VNA) (PNA-L N5230C, Agilent), controlled with custom MATLAB programming, to measure the

transmission spectrum of the resonator board. The transmission coefficient was measured as S_{21}, which is a complex vector quantity whose magnitude, $|S_{21}|$, is equal to the ratio of the voltage wave amplitude at the output to that input to the device.

We found that a lower input power produced a narrower transmission resonance (Figure 4.1b), but also increased noise. In all measurements, the input microwave power from the VNA to the sensor was -50 dBm (0.01 μW). This was achieved with the combination of attenuators both external to and internal to the VNA.

We sampled 301 evenly spaced frequencies in the specified band of each measurement and maintained this number for all measurements. Maintaining a constant sampling number across measurements ensured a consistent spectrum sampling rate: in each of our measurements, the transmission spectrum was recorded 5 times per second (every 0.2 s). A consistent sampling rate was required for an accurate analysis, and a sampling rate greater than 2 Hz was necessary to capture the insect movements, which were often observed to occur in time scales shorter than 1 s.

Occasionally, insect movements produced spectrum shifts greater than the monitored bandwidth. In these cases, the bandwidth was increased to capture all spectrum shifts. The largest bandwidth monitored in a measurement was 10 MHz; the smallest measurements captured a bandwidth of 2 MHz.

The sensor and all power and RF cables were fixed to an optical table to minimize the influence of vibrations on the signal. A dielectric plate with a kernel-shaped slot was fixed flat to the sensor to ensure that kernels were placed on the same part of the resonator so that the data reflected variations in insect behaviour instead of variations in the electric field profile of the resonator. For an individual measurement of insect activity, we placed the insect-bearing wheat kernel crease-side down onto the sensor. To block external wireless signals, the sensor was shielded with microwave-absorbing material (C-RAM LF-77, Cummings Microwave). The shielding was also opaque to visible light.

We conducted observations of kernels bearing *S. oryzae* in the larval, pupal, and adult

stages. As control measurements, we also tested the following: non-insect-bearing kernels, kernels with dead insects (terminated by freezing), empty kernels from which the adults had previously emerged, and the case when no kernel was placed on the sensor. In all control measurements, the result was the same, and a typical spectrogram is shown in Figure 4.2a.

All measurements were conducted at a room temperature of about 23 °C.

4.2.2 Sensor design and fabrication

The resonator constituting the sensor was made from microstrip transmission line. Microstrip line consists of a flat conductor separated from a ground plane by a dielectric (insulating) layer. The resonator was modelled and simulated using CAD software (CST Studio Suite, Computer Simulation Technology GmbH). The microstrip structure was then milled from a copper clad, double sided, FR-4 grade laminate (Part no. 106397, LPKF Laser & Electronics) using a computer-controlled circuit board plotter (Protomat S103, LPKF Laser & Electronics). The board substrate and copper cladding had thicknesses of 1.5 mm and 35 μm, respectively. Finally, the electrical components comprising the regenerative element and the external connectors were hand-soldered to the structure to complete the sensor. The addition of the regenerative element decreases the width of the transmission resonance by a factor of approximately 10^2 [19, 32].

The transmission spectrum of the finished resonator is shown in Figure 4.1b. It consists of two peaks. Only the broader, high-frequency peak was stable in both height and width. The narrow, low-frequency peak is a discrete spurious signal, and was unstable. The spurious signal may have been caused by intermodulation products resulting from non-linearities in the amplifier [24]. In our analysis, we examined only the centre of the broad peak, f_0. We found that the spurious signal had little effect on the fitting procedure used to obtain f_0 because its distance from the main peak is large relative to the width of both peaks. As different kernels were placed on the sensor, the steady-state position of f_0 would vary between 3.76 GHz and 3.83 GHz, depending on the individual features of each kernel such

as the size, shape, and moisture content. The size of the insect and the cavity it created could also affect the steady-state position of f_0.

The fixture to hold the kernels in place on the resonator during measurements was modelled and cut using the same process. It was then fixed to the resonator board with brass screws. Fixing the board to the resonator induced a one-time shift in f_0, but did not introduce additional noise.

4.2.3 Insect rearing and classification

Sitophilus oryzae obtained from colonies maintained in the lab, originally taken from a flour mill in the province of Manitoba, Canada, were used in this study. The colonies were reared at 30 ± 1 °C and 70 ± 5% relative humidity (rh) at dark. To obtain kernels bearing insects, approximately 1000 adults were introduced to a jar containing 2 kg of rearing medium. The rearing medium was whole hard red spring wheat kernels (14% MC [ASABE, 2009]). The jar was kept at the same rearing conditions as the parent colony for 48 h to allow the adults to lay eggs. The adults were then separated from the rearing medium using a sieve with 1.651 mm apertures. To obtain kernels bearing larvae, pupae, and adults, kernels were retrieved from the jar after 10, 23, and 28 d, respectively. Infestation status was visually examined using a soft X-ray imaging system (MX-20, Faxitron Bioptics, LLC).

4.2.4 Detection statistics analysis

To obtain the centre of the transmission resonance, f_0, (Figure 4.1b) we used the MATLAB fit function to fit the Gaussian $|S_{21}| = A\exp[-(f - f_0)^2/c^2] + d$ to the recorded spectra, with the independent variable being the frequency, f, and the dependent variable being $|S_{21}|$ (as seen in Figure 4.1b), with A, c, and d corresponding to the peak height, width, and vertical offset, respectively, though these last three variables were not considered in the final analysis. The width, c, was kept constant during fitting. This process consistently extracted the centre of the transmission resonance peak (Figures 4.1b, 4.2).

On the f_0 data, we performed two analyses: one to study the variation of measured activity levels, and one focussed on insect detection based on derivative thresholding. The latter analysis is referred to as the derivative threshold analysis in this report.

In the analysis of the activity level variation, we computed the first time-derivative of f_0, df_0/dt, for each measurement. Because the data were discrete samplings of f_0, the derivative at time t was approximated numerically as $f_0'(t) = [f_0(t + \Delta t) - f_0(t)]/\Delta t$ where the time step Δt = 0.2s was constant across all measurements. Then, all f_0' points were combined according to developmental stage and binned into histograms, as shown in Figure 4.3. To reduce noise in f_0, we used a 10-point (2 s) moving average filter prior to this analysis. For this analysis, all measurements were truncated to 10 minutes to ensure that each had the same statistical weight.

In the derivative threshold analysis, we studied the detection probability as it varied with the length of observation. This analysis required a quantitative definition of insect activity based on the observed signal. In the absence of any disturbance, the sensor output was relatively constant; occasionally, slow changes in the ambient conditions would cause f_0 to drift slowly. In contrast, the sensor response to insect activity was characterized by rapid changes in f_0. Therefore, we looked at f_0', as an indicator of activity. We then defined positive detection as instances when the magnitude of f_0' exceeded a prescribed threshold (11.7kHz/s). We selected the threshold such that no detections were registered from our control data (measurements of kernels without live insects). To reduce noise in f_0, we used a 10-point (2 s) moving average filter prior to this analysis.

The next step was to calculate the detection fraction — the fraction of measurements in which an insect was detected — as it varied with observation length and insect stage. First, we truncated all measurements to 10 minutes. We then divided the measurements into equally sized time intervals to simulate short duration observations from our measurements. We combined all our measurements, grouping them by developmental stage, and counted the fraction of the intervals in which f_0' exceeded the defined threshold to estimate the probability

of detection. We repeated this procedure for interval widths of 5, 10, 30, 60, 120, 180, 240, 300, and 600 s for each stage of *S. oryzae*. The number of individuals tested at each stage are as follows: 73 larvae, 35 pupae, 44 adults, and 70 control measurements (measurements without live insects). This analysis treated the activity of a given individual as a random occurrence in the time scale of our observations.

4.3 Results & Discussion

4.3.1 Real-time activity monitoring

Figure 4.2 shows typical transmission spectrograms we obtained from kernels without insects (Figure 4.2a-c) and kernels bearing the three developmental stages of *S. oryzae*: larva (Figure 4.2d-f), pupa (Figure 4.2g-i), and adult (Figure 4.2j-l).

Each insect stage was unique not only in their frequencies of activity, but also the signal patterns they created. Adults were the most active and typically showed near-constant activity of varying intensity. With larvae, we observed periods of inactivity punctuated by bursts of activity and short, sudden movements. Pupae were the least likely to be active during measurement. With sound kernels, the spectrum was steady, and the only changes observed were slow thermal drifts in some cases.

The observed activity agrees with our knowledge of the *S. oryzae* life cycle. To interpret the observed spectrogram patterns in terms of the behaviour inside kernels, we draw from the x-ray radiograph study of *S. oryzae* performed by Sharifi and Mills [42]. The known activities of *S. oryzae* larvae include feeding (which simultaneously bores out the cavity), defecating, moulting, and resting. Larvae will also construct the pupal chamber in the final 1-2 days before pupation. Regular patterns, such as in Figure 4.2f, may reflect a correspondingly regular motion of the larva, such as boring or moulting. Pupae, on the other hand, were expected to show little activity: they do not feed, defecate, or moult until eclosion. However, they do still move: by moving their abdomens, pupae sometimes rotate in their chambers,

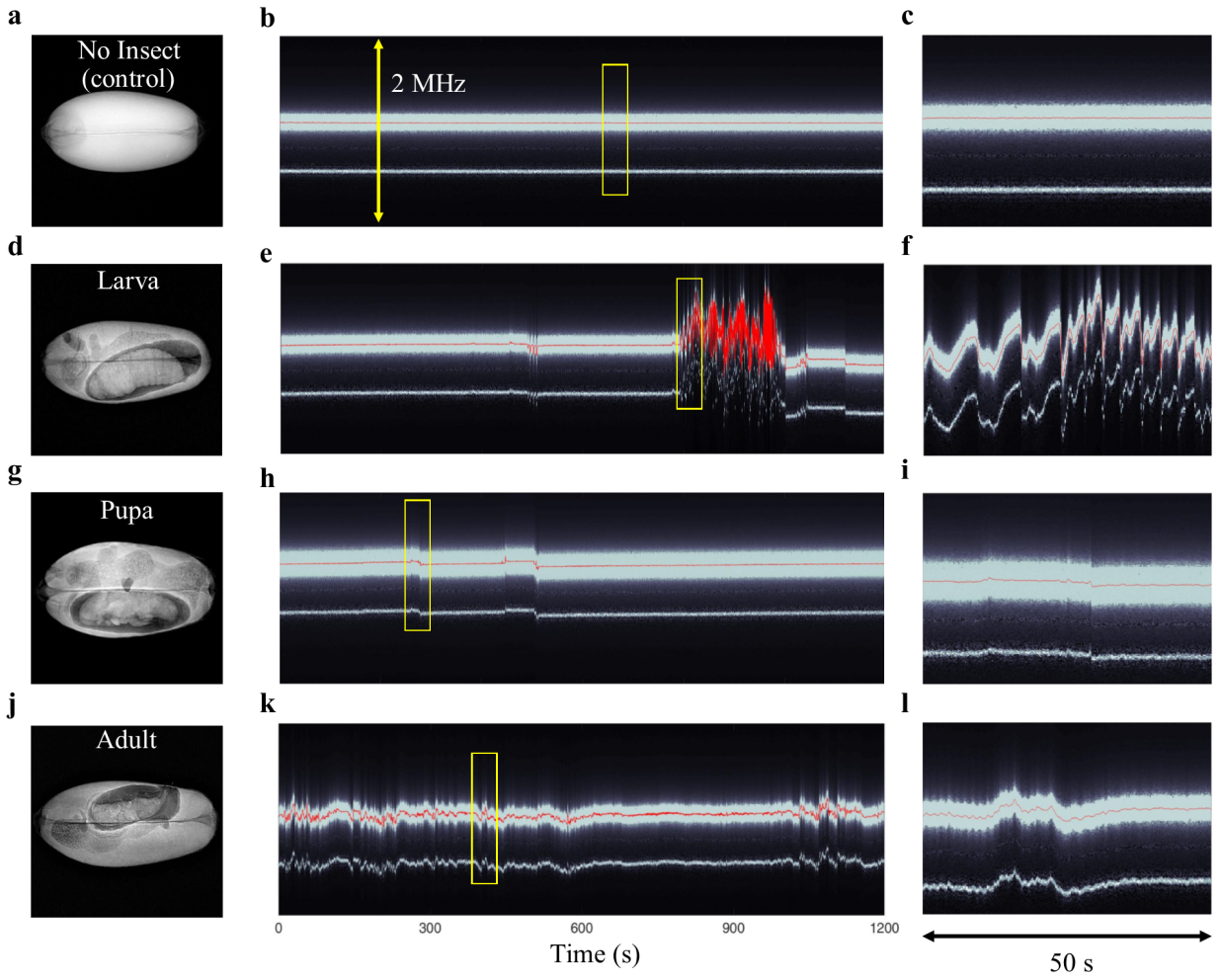

Figure 4.2: Transmission spectrograms of the resonator demonstrating the varied patterns measured from wheat kernels infested with Sitophilus oryzae. The peak centre, obtained by fitting to the spectrum, is also shown as a red line. We used X-ray imaging to identify the developmental stages of each individual tested. (a) An x-ray radiograph of a sound wheat kernel, which we used as a control. (b) A spectrogram we recorded when a kernel without internal insects was placed on the resonator. (c) Expanded view of the spectrogram. (d – f) The same for a larva-infested kernel, (g – i) a pupa-infested kernel, and (j - l) an adult-infested kernel.

which could explain why signals were still observed in pupae. Adults spend 3-4 days in the kernel waiting for their cuticle to harden before emerging. However, they have several movable appendages: legs, antennae, elytra, and a snout, the movement of which may be the source of the weak but regular and rapid spectrogram patterns as seen in Figures 2 k-l. Adults will also rotate in the chamber to best align themselves for emergence. Additionally,

they will be very active as they begin to emerge.

The examples shown in Figure 4.2 are representative of the results, but variations among individuals of the same stage were also observed. Figure 4.3 summarizes the variability of approximated first time-derivative of f_0, f_0', in our measurements for the insect stages tested. The derivative was approximated by computing the difference between adjacent points and dividing by the time step (§4.2).

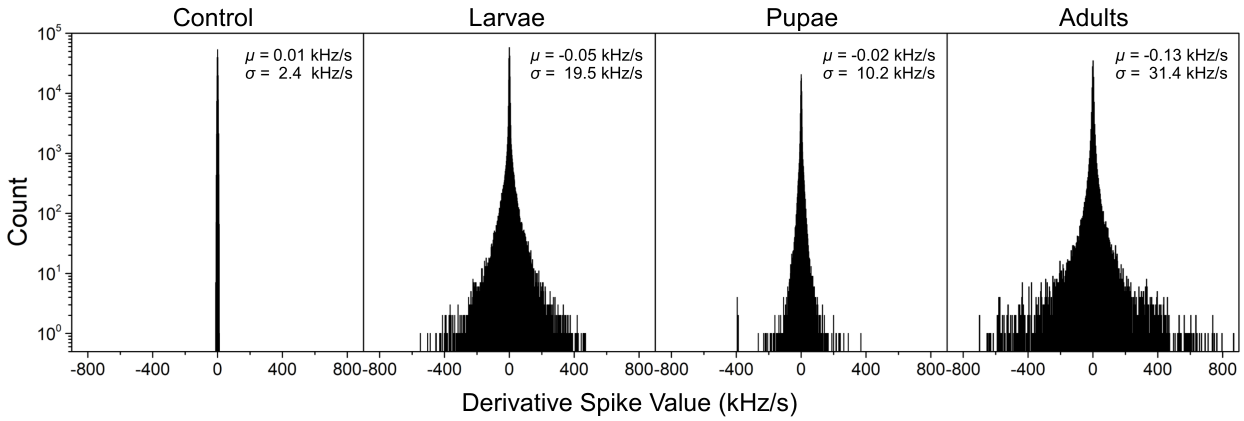

Figure 4.3: The distribution of the values of the measured derivative spikes in our control measurements and measurements of kernels infested with each developmental stage of *S. oryzae*. Note the logarithmic vertical scale. μ and σ correspond to the calculated mean and standard deviation, respectively

We observed significant variability in the activity levels of the insects. The test group that showed the least variability was the control group (no live insects inside the kernel). It is seen from Figure 4.3 that there is a clear distinction in activity levels measured when insects are present versus the control. Furthermore, there is a markedly lower variability (standard deviation) in f_0' among the control measurements; controls showed a consistently low noise level. The reason for variations in the noise level may be slow drifts caused by changes in the ambient air temperature.

The maximum f_0' observed in the control group was 11.67 kHz/s. This value exceeded the maxima of some measurements in the insect groups. As a result, we can expect any detection method that relies solely on the thresholding of a measure of activity to produce

either false positive or false negative results. In fact, this limitation is apparent in the derivative threshold section, and is a motivation to turn to a more sophisticated analysis, such as machine learning.

4.3.2 Derivative thresholding technique

The ability of the sensor to non-intrusively detect insects inside kernels could prove useful for pest-management when screening grain samples. To study this application, we characterized the sensor for binomial (absence-presence) trials of wheat kernels for internal *S. oryzae*. We sought to study how observation duration affected detection probability. We accomplished this by simulating different observation times on our data by dividing it into intervals and calculating the fraction of intervals in which activity was detected, as described in the Methods. Specifically, we examined the use of the first time derivative of f_0, f_0', as an indicator of insect activity.

In this method, detection is counted when intervals have at least one spike in f_0' exceeding a threshold of 11.7 kHz/s, which was selected based on the results shown in Figure 4.3. Naturally, longer measurements are more likely to capture spikes in f_0' exceeding the threshold. Figure 4.4 illustrates with a single measurement how the fraction of all intervals in which activity is detected increases with the size of the interval. We see that only intervals having rapid changes in f_0 indicate a detection and that no detections are registered when f_0 is steady. This also illustrates the fundamental limitation of the sensor: ultimately, detection depends on insect movement.

Figure 4.5 shows the detection fraction as it varies with interval size and insect type. As expected, the detection fraction increased with the interval width, which simulates observation length. Of the insects detected, it took an average of 2 min for a detection to be recorded, and 83% of insects were detected within 10 minutes. For any given interval width, the insect stages in order of highest to lowest detection fraction is generally as follows: adults, larvae, and pupae. This agrees with our qualitative understanding of the behaviour

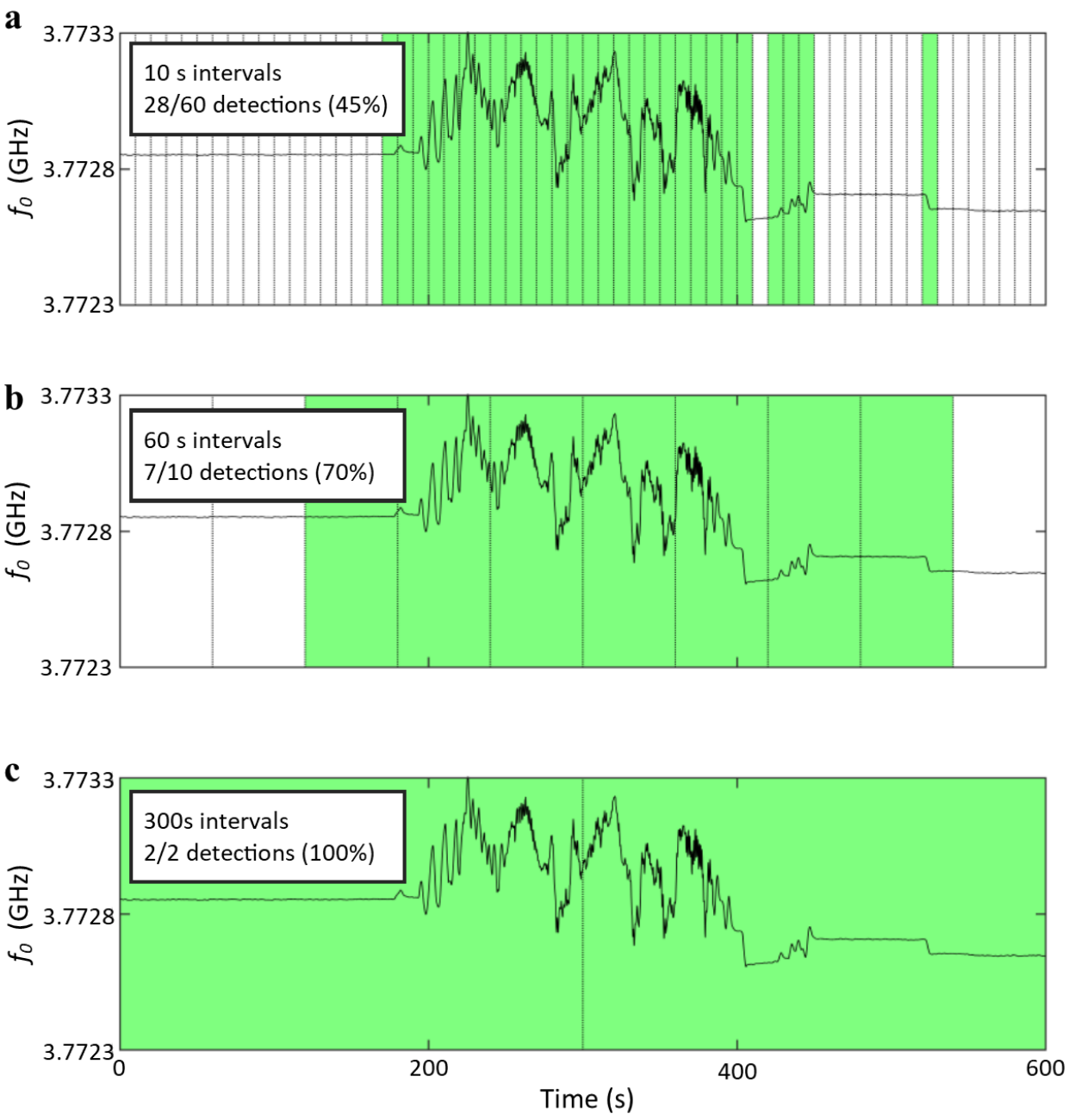

Figure 4.4: A demonstration of how the probability of detection depends on the observation duration in the example measurement shown in Figure 4.2e. The plotted lines are the resonance peak centre, f_0, (obtained through fitting), smoothed using a 10-point (2 s) moving average filter. The measurement is divided into equally sized intervals, and each interval is tested for activity. Intervals in which the first time-derivative of f_0 exceeds the prescribed threshold (11.7 kHz/) are highlighted. (a) The measurement divided into 10 s intervals. (b) 60 s intervals. (c) 300 s intervals.

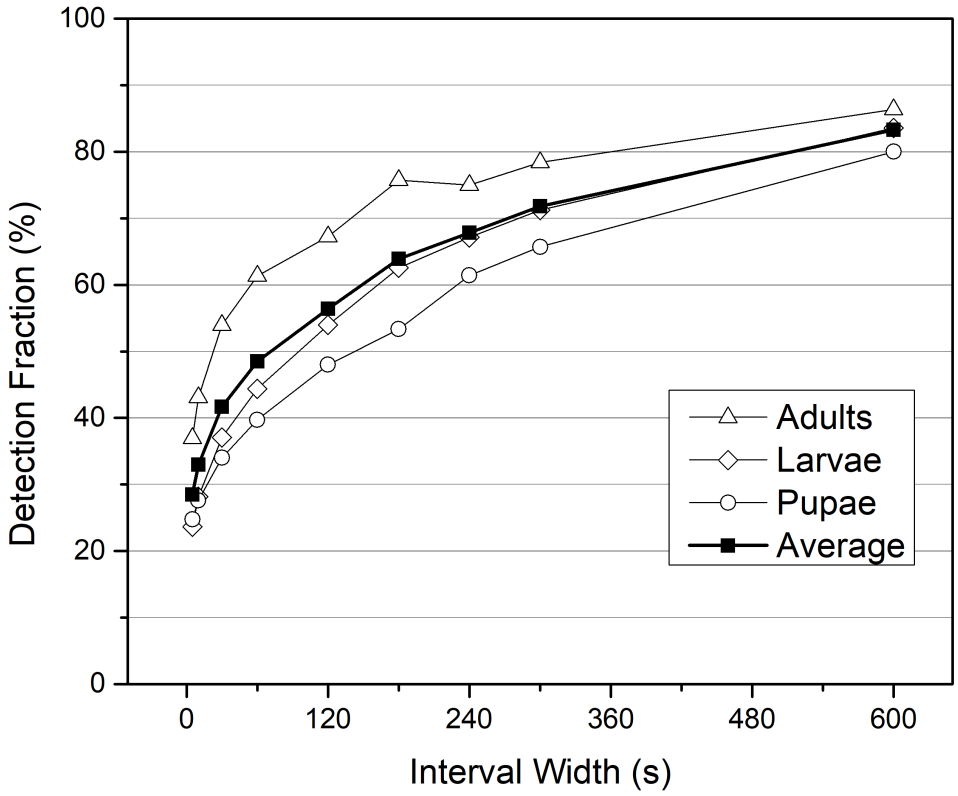

Figure 4.5: The fraction of all intervals in which a detection was recorded as it changed with observation time (interval width). The average is across the arithmetic mean across the 3 developmental stages tested.

of insects inside kernels, as described in the previous section. Quantitatively, the results also follow the expectations suggested by the data in Figure 4.3.

Since the measured activity levels of some insects tested fell below the maximum noise level measured in the controls, the derivative thresholding technique might fail to detect them, especially if the insects do not move during the observation period. This is the fundamental limitation of the system; it cannot detect insects if they do not move. As a result, the detection probability does not reach 100%.

4.4 Conclusions

4.4.1 Summary

The work presented in this chapter demonstrated that the detection of insects inside wheat kernels is possible when using a sensor having an active resonator as the central component. When kernels bearing insects were placed on the sensor, we observed shifts in the resonance frequency which did not occur when kernels without insects were placed on the sensors. The shifts observed likely correspond to the movements of the insect inside the kernel. We tested several kernels with insects in the larval, pupal, and adult stages of *Sitophilus oryzae* and observed distinct differences between the activity levels of each stage. We also observed patterns in the frequency shifts which may be indicative of the developmental stage of the insect inside the kernel. We developed an analysis to ascertain the presence of insects inside kernels from the first time-derivative of the resonance frequency. We simulated the performance of this analysis for observation periods ranging from 5 s to 600 s, and found that the detection rate increased generally with observation time, with the average detection rate being roughly 30% with 5 s observations and roughly 80% with 10 min measurements. Of the insects detected, it took an average of 2 min for a detection to be recorded.

4.4.2 Future Work

The technique demonstrated in this chapter has the potential to be used in a grain sample testing system where samples pulled from a large bulk of grain are tested for insects. With an average detection rate of 80% in 10 min measurements, this system could be used in grain elevators as a replacement for the Berlese Funnel, which takes 5 - 6 h to process a sample and has an efficiency lower than 80% [3]. However, before the microwave sensor system could compete with the Berlese funnel, it would have to be developed into a system which can process up to 1 kg of grain at a time. In Chapter 3.7, it was seen that the range of the

sensor in grain is only a few centimetres. To be able to process a large amount of grain, it would then be necessary to increase the sensing surface of the sensor so that the grain sample could be spread into a layer which can be fully penetrated by the sensor. This would likely require the integration of multiple microwave sensors in a single device. To this end, future work on this project would investigate the interactions between interconnected active resonators, eliminate dead regions on the device which do not have the sensitivity to detect insects by closely spacing the resonators, and characterize the sensing range of the resonators for different grain types and moisture contents as well as for different types of insect pests.

5

CONCLUSIONS

5.1 Summary

This thesis presented new sensors for the purpose of stored-grain insect detection. These sensors have as their central component active microwave resonators. Active resonators incorporate an active circuit component which compensates energy loss in the resonator, which results in a high Q-factor (15,200) and an extremely narrow (0.25 MHz FWHM at 3.8 GHz) resonance. This allows insect activity in grain – both inside and outside of the kernels – to be detected from the shifts in the resonator frequency, a capability which was demonstrated by experiment.

The key mechanism of the sensor lies in the sensitivity of the propagation characteristics of the transmission line constituting the active resonator. Since the electric and magnetic fields of the resonator are largely situated in open air, they form a sensing volume. Changes to the fields, caused by the introduction of objects or changes in said objects, alter the propagation of microwaves in the resonator and trigger shifts of the resonance frequency. In the application of insect detection, shifts in the resonance frequency are caused by the movement of insects through the fields. The work presented in Chapters 3 and 4 demonstrate the ability of the sensor to detect the movement of insects moving among the kernels in a

grain sample, and the movement of insects hidden inside the grain kernels.

In the work presented in Chapter 3, it was established that the active resonator sensor could in fact detect the movement of insects. This was done by placing adult *Triboleum casteneum* and *Cryptolestes ferrugineus* directly onto the surface of the resonator and allowing them to move freely within an enclosed area surrounding the active resonator. It was observed that the insects indeed caused the resonance frequency of the resonator to shift and that the magnitude of the shift depended on the size of the insect. Next, by using temperature to influence insect activity, it was shown that the level of variation in the signal recorded from the sensor was indicative of the amount of movement in the sensing area. However, the signal was also confounded by the size and range of the insects. Finally, the concept of using the sensor to detect insects in small grain samples was proved. This last experiment demonstrated that the active resonator maintained its sharp resonance even with the added dielectric loss caused by the wheat. The sensor was therefore able to detect insect movement in the grain sample.

The work presented in Chapter 4 demonstrated that the detection technique could be extended to insects hidden inside kernels. This was achieved by placing wheat kernels bearing *Sitophilus oryzae* on the surface of the sensor and recording the sensor output over several minutes. This procedure was repeated with kernels bearing *S. oryzae* larvae, pupae, and adults, and compared the results to those obtained from uninfested kernels. Measurements of over 30 individuals from each group were collected. It was found that not only was insect movement detected inside kernels, but that each development stage of *S. oryzae* exhibited different activity levels. It was also discovered that each stage produced unique patterns of frequency shifts, which may reflect each stage's behaviour. By using a thresholding technique, which tested the time-derivative of the resonance frequency, the presence of insects inside kernels at every development stage was ascertained. This technique was tested with observation times ranging from 5 s to 10 min and it was found that the fraction of measurements which successfully detected insects increased from 30% with 5 s measurements to 80%

with 10 minute measurements, on average. These results may inform the design of future sample testing systems.

5.2 Outlook

The sensors presented in this thesis are still at an early stage of development. Much more work needs to be done to develop them into useful industrial systems. Regarding research and development, there are two general applications in which the sensors might be implemented. One is the monitoring of insect populations in grain storage bins; the other is the testing of grain samples pulled from a bulk.

In the monitoring of grain storage bins, the sensors could be placed in the bins and connected by cables to an external computer from which the sensor outputs could be read. The effectiveness of this system would rely on the insects moving close enough to the sensors to trigger a measurable shift in the resonance frequency. For this reason, detection would be limited to external insects; it would not be effective in detecting internal insects because they do not move throughout the grain bulk. Since the range of the sensors is limited to only a few centimetres, several sensors would have to be placed in the bin to cover a useful fraction of the grain bulk. Before the sensors can be implemented in this way, the performance of the sensor in a bulk grain environment would have to be studied. This includes studies of ambient noise, studies of environmental effects such as changes in moisture and temperature, and studies of how insect population density affect the likelihood of detection.

In the application of grain sample testing, the focus of detection would be on internal insects. External insects in the sample could easily be shaken out, but internal insects are difficult to identify and separate from the grain. An example of a sample-testing system might have a surface composed of multiple sensors, upon which a grain sample could be spread. Spreading the sample into only a few layers of grain would overcome the limited range of the sensor and allow larger samples to be tested. To better understand how the sensor

could be implemented in such a system, future studies will examine the interactions between interconnected active resonators, the sensing range of the resonators, and the performance of the system when used to test grains other than wheat and insects other than *S. oryzae*.

Through this project, our group has established interdisciplinary collaborations with researchers from different institutions. We have new relationships with the Department of Biosystems Engineering at the University of Manitoba and Agriculture and Agri-Food Canada which has combined our expertise and resources with theirs in agriculture, grain storage, and entomology. Furthermore, this project has attracted the interest of a group from the National Research Council specializing in machine learning. This group has helped us explore and improve methods to analyse with machine learning the signal obtained from the sensors. We have caught the interest of the private sector too: OPIsystems Inc., a Calgary-based firm specialising in grain storage technology, has expressed interest in joining the project. At the time of writing, the CEO of OPIsystems Inc. has scheduled to meet with us in person to receive a demonstration of the technology and discuss future collaboration. We are also in the process of applying for patent protection for this technology.

BIBLIOGRAPHY

[1] D. Kumar and P. Kalita, "Reducing postharvest losses during storage of grain crops to strengthen food security in developing countries," *Foods*, vol. 6, no. 8, 2017.

[2] D. Hagstrum and B. Subramanyam, *Fundamentals of Stored-Product Entomology*. St. Paul, Minnesota, USA: AACC International, 2006.

[3] L. B. Smith, "Efficiency of Berlese-Tullgren funnels for removal of rusty grain beetles, *Cryptolestes ferrugineus*, from wheat samples ," *The Canadian Entomologist*, vol. 109, no. 4, pp. 503–509, 1977.

[4] S. Neethirajan, C. Karunakaran, D. Jayas, and N. White, "Detection techniques for stored-product insects in grain," *Food Control*, vol. 18, no. 2, pp. 157–162, 2007.

[5] D. Hagstrum, J. Webb, and K. Vick, "Acoustical detection and estimation of *Rhyzopertha dominica* (f.) larval populations in stored wheat," *Florida Entomologist*, pp. 441–447, 1988.

[6] R. Mankin and A. Moore, "Acoustic detection of *Oryctes rhinoceros* (coleoptera: Scarabaeidae: Dynastinae) and *Nasutitermes luzonicus* (isoptera: Termitidae) in palm trees in urban guam," *Journal of Economic Entomology*, vol. 103, no. 4, pp. 1135–1143, 2010.

[7] T. Pearson, D. Brabec, and C. Schwartz, "Automated detection of internal insect in-

festations in whole wheat kernels using a perten skcs 4100," *Applied Engineering in Agriculture*, vol. 19, no. 6, pp. 727–733, 2003.

[8] T. Pearson and D. L. Brabec, "Detection of wheat kernels with hidden insect infestations with an electrically conductive roller mill," *Applied Engineering in Agriculture*, vol. 23, no. 5, pp. 639–646, 2007.

[9] J. Chambers, N. McKevitt, and M. Stubbs, "Nuclear magnetic resonance spectroscopy for studying the development and detection of the grain weevil, *Sitophilus granarius* (l.)(coleoptera: Curculionidae), within wheat kernels," *Bulletin of entomological research*, vol. 74, no. 4, pp. 707–724, 1984.

[10] AACC International, *Cracking-Flotation Test for Internal Insects in Whole Grains, AACCI Method 28-22.02*. Approved Methods of the American Association of Cereal Chemists, 11 ed., 1999.

[11] F. E. Dowell, J. E. Throne, and J. E. Baker, "Automated nondestructive detection of internal insect infestation of wheat kernels by using near-infrared reflectance spectroscopy," *Journal of Economic Entomology*, vol. 91, no. 4, pp. 899–904, 1998.

[12] R. Haff and D. Slaughter, "Real-time x-ray inspection of wheat for infestation by the granary weevil, sitophilus granarius (l.)," *Transactions of the ASAE*, vol. 47, no. 2, pp. 531–537, 2004.

[13] C. Karunakaran, D. Jayas, and N. White, "Soft x–ray inspection of wheat kernels infested by *Sitophilus oryzae*," *Transactions of the ASAE*, vol. 46, no. 3, p. 739, 2003.

[14] H. Tang, S. Kaur, L. Fu, B. Yao, X. Li, H. Gong, Y. Gui, and C.-M. Hu, "Life signal detection using an on-chip split-ring based solid state microwave sensor," *Applied Physics Letters*, vol. 105, no. 13, p. 133703, 2014.

[15] R. W. Mankin, "Microwave radar detection of stored-product insects," *Journal of Economic Entomology*, vol. 97, no. 3, pp. 1168–1173, 2004.

[16] M. Skolnik, *Introduction to Radar Systems*. London: McGraw-Hill Inc., 2 ed., 1980.

[17] B. Yao, Y. Gui, J. Rao, S. Kaur, X. Chen, W. Lu, Y. Xiao, H. Guo, K.-P. Marzlin, and C.-M. Hu, "Cooperative polariton dynamics in feedback-coupled cavities," *Nature Communications*, vol. 8, no. 1, p. 1437, 2017.

[18] G. A. Ferrier, S. F. Romanuik, D. J. Thomson, E. Bridges, and M. R. Freeman, "A microwave interferometric system for simultaneous actuation and detection of single biological cells," *Lab on a Chip*, vol. 9, pp. 3406–3412, 2009.

[19] M. Nick and A. Mortazawi, "Low phase-noise planar oscillators based on low-noise active resonators," *IEEE Transactions on Microwave Theory and Techniques*, vol. 58, no. 5, pp. 1133–1139, 2010.

[20] M. H. Zarifi and M. Daneshmand, "Non-contact liquid sensing using high resolution microwave microstrip resonator," in *Microwave Symposium (IMS), 2015 IEEE MTT-S International*, pp. 1–4, IEEE, 2015.

[21] S. Ramo, J. R. Whinnery, and T. Van Duzer, *Fields and Waves in Communications Electronics*. New York: John Wiley and Sons, Inc., 3 ed., 1994.

[22] R. E. Collin, *Foundations for microwave engineering*. New York: McGraw-Hill Inc., 1 ed., 1966.

[23] T. C. Edwards, *Foundations for Microstrip Circuit Design*. New York: John Wiley and Sons, Inc., 1981.

[24] D. Pozar, *Microwave Engineering*. Hoboken, NJ, USA: John Wiley and Sons, Inc., 4 ed., 2012.

[25] E. O. Hammserstad, "Equations for microstrip circuit design," *Proc. European Microwave Conference*, pp. 268–272, 1975.

[26] Agilent Technologies, *Network Analyzer Basics*. Santa Clara, CA, USA, 2004.

[27] Anritsu Corporation, *Vector Network Analyzer Primer*. Morgan Hill, CA, USA, 2009. Appl. Note 935 11410-00387.

[28] Rohde & Schwarz USA, Inc., *Network Analyzer Basics*. Columbia, MD, USA, 2015.

[29] National Instruments Inc., *Introduction to Network Analyzer Measurements: Fundamentals and Background*. Austin, TX, USA, 2018.

[30] A. Verma and A. Omar, "Microstrip resonator sensors for determination of complex permittivity of materials in sheet, liquid and paste forms," *IEE Proceedings-Microwaves, Antennas and Propagation*, vol. 152, no. 1, pp. 47–54, 2005.

[31] Y. Yang, H. Zhang, J. Zhu, G. Wang, T.-r. Tzeng, and X. Xuan, "Distinguishing the viability of a single yeast cell with an ultra-sensitive radio frequency sensor," *Lab on a Chip*, vol. 10, pp. 553–555, 2010.

[32] M. H. Zarifi, S. Farsinezhad, K. Shankar, and M. Daneshmand, "Liquid sensing using active feedback assisted planar microwave resonator," *IEEE Microwave and Wireless Components Letters*, vol. 25, no. 9, pp. 621–623, 2015.

[33] D. W. Hagstrum, P. W. Flinn, and D. Shuman, "Automated monitoring using acoustical sensors for insects in farm-stored wheat," *Journal of Economic Entomology*, vol. 89, no. 1, pp. 211–217, 1996.

[34] Rogers Corporation, "Data sheet for DiClad Series laminates," 2017.

[35] ASABE, *Standard S352.2: Moisture measurement - Unground grain and seeds*. St. Joseph, MI, USA: ASABE, 2014.

[36] R. Mahroof, B. Subramanyam, J. E. Throne, and A. Menon, "Time-mortality relationships for *Tribolium castaneum* (Coleoptera: Tenebrionidae) life stages exposed to elevated temperatures," *Journal of Economic Entomology*, vol. 96, no. 4, pp. 1345–1351, 2003.

[37] G. D. Arlene-Christina, D. S. Jayas, P. G. Fields, F. Jian, N. D. G. White, and K. Alagusundaram, "Movement of *Cryptolestes ferrugineus* out of wheat kernels and their mortalities under elevated temperatures," *Journal of Stored Products Research*, vol. 59, pp. 292–298, 2014.

[38] F. Jian, P. G. Fields, K. Hargreaves, and D. S. Jayas, "Chill-coma and minimum movement temperatures of stored-product beetles in stored wheat," *Journal of Economic Entomology*, vol. 108, no. 5, pp. 2471–2478, 2015.

[39] F. Jian, D. S. Jayas, and N. D. G. White, "Movement of *Tribolium castaneum* (Coleoptera: Tenebrionidae) adults in response to temperature gradients in vertical and horizontal wheat and corn columns," *Journal of Economic Entomology*, vol. 98, no. 4, pp. 1413–1419, 2005.

[40] F. Jian, D. S. Jayas, N. D. G. White, and W. E. Muir, "Temperature and geotaxis preference by *Cryptolestes ferrugineus* (Coleoptera: Laemophloeidae) adults in response to 5 °C / m temperature gradients at optimum and hot temperatures in stored wheat and their mortality at high temperature," *Environmental Entomology*, vol. 31, no. 5, pp. 816–826, 2002.

[41] F. Jian, D. S. Jayas, and N. D. G. White, "Movement of adult rusty grain beetles, *Cryptolestes ferrugineus* (Coleoptera: Cucujidae), in wheat in response to 5 °C / m temperature gradients at cool temperatures," *Journal of Stored Products Research*, vol. 39, pp. 87–101, 2003.

[42] S. Sharifi and R. B. Mills, "Developmental activities and behavior of the rice weevil

inside wheat kernels," *Journal of Economic Entomology*, vol. 64, no. 5, pp. 1114–1118, 1971.